

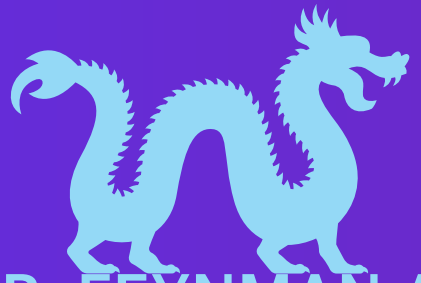


# JOSEPHSON-BASED QUANTUM PROCESSOR DESIGN



Lucas Camponogara Viera

# PREREQUISITES



## MR. FEYNMAN AND THE SHAMBLES OF TAIWAN



"NO BODY UNDERSTANDS QUANTUM MECHANICS."  
—FEYNMAN, R.



# THE ROAD BEHIND



- E-beam Lithography**
- Optical Lithography**
- Superconductivity**
- Quantum Information Theory**
- Classical Information Theory**
- Microwave Transmission Line Theory**
- Electromagnetic Theory**

# OUTLINE

- 1. Physical Constraints: allowed temperatures, materials, and op. frequency;**
- 2. Building Blocks: waveguide resonators, capacitors, inductors, josephson tunnel junction;**
- 3. Qubit-cavity Coupling: qubit control (superposition) and readout (cQED: Jaynes-Cummings model);**
- 4. Qubit-Qubit Coupling: entanglement (cQED: Dicke model);**
- 5. Processor Design: pyEPR;**
- 6. Processor Simulation: scQubits, and pyEPR+Ansys HFSS;**
- 7. Fabrication process: photolithography, and e-beam lithography;**
- 8. Quantum Process Tomography: gate fidelity (channel noise).**

# QUBIT PLATFORMS

# QUANTUM EMBODIMENTS

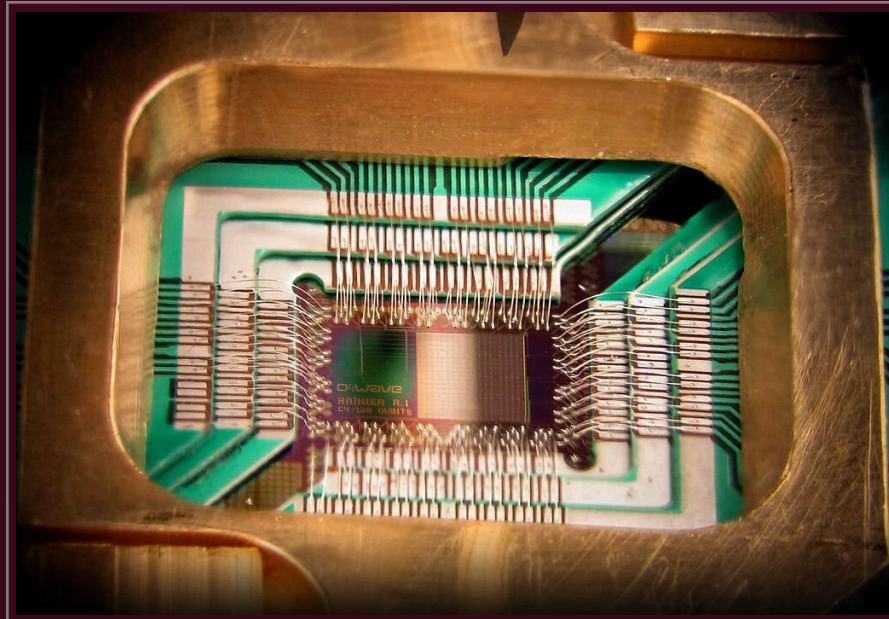
Liquid state NMR QC; ion trap QC; quantum dot QC; harmonic oscillator QC; heteropolymer QC; cluster- state QC; topological or anyon-based QC; optical photon; and nonlinear optical media QC; QC based on semiconductors spins; and superconducting QC based on circuit quantum electrodynamics (circuit QED). Those of skill in the art will also appreciate that a quantum processor may be embodied in a system other than those described above.

Type	Scaled CMOS (classical)	Ion trap	Quantum dot	Optical circuit	Gate-based superconducting circuit	Superconducting circuit (adiabatic computation)
State variable	Electrical charge	Ion spin	Electron spin, energy level, or position	Photon polarization, time, or position	Magnetic flux, charge, or current phase	Magnetic flux
Material	Doped silicon	Atoms in free-space electromagnetic field	Solid-state semi-conductor at cryogenic temperatures	Optical waveguides, for example, etched in silicon	Superconducting Josephson junction at cryogenic temperatures	Superconducting Josephson junction at cryogenic temperatures
Device gate	MOSFET	Laser- or vibrational-mediated interaction	Laser- or electrically-driven exchanges and rotations	Beam splitters and photon detectors	Electrically-driven exchanges and rotations	Electrically-controlled couplers
Maximum demonstrated variables	> $10^9$ transistors per chip, $\approx 10^{16}$ per supercomputing system	14	3	8	2 full qubits + 2 special-purpose memories	8 coupled, 50 functional?

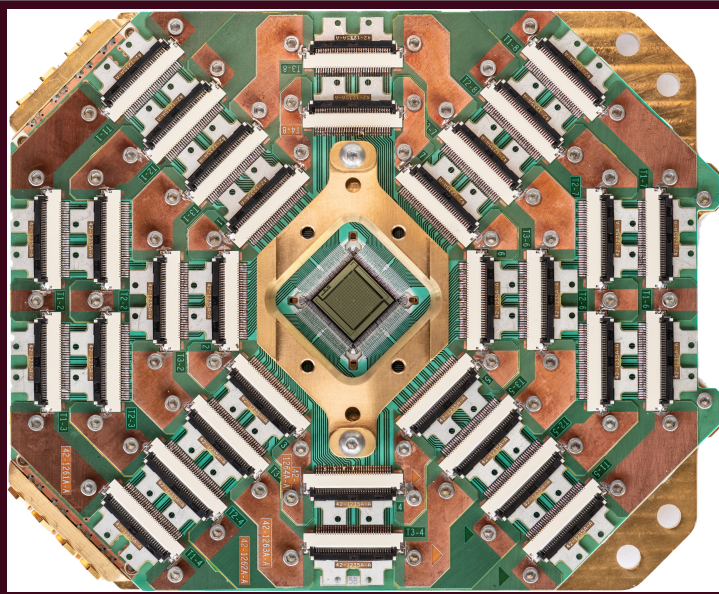
## Annealing System

### Ising Model

D-Wave One (Rainier) 128-qubits



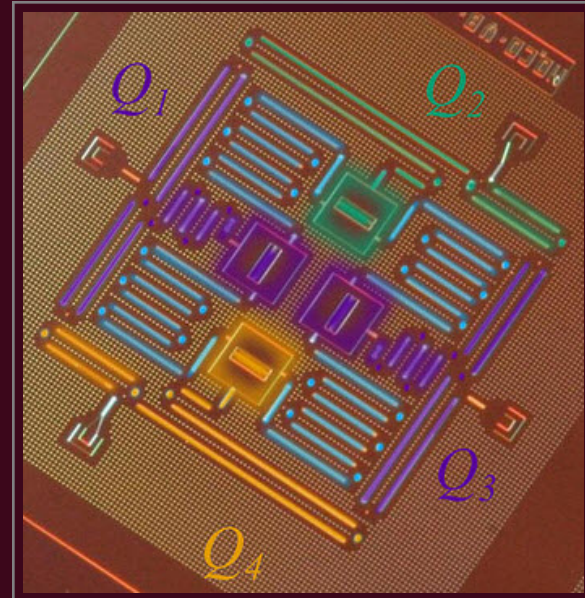
D-Wave Advantage  
5000-qubits &  $>1\text{M J}_\text{J}$ .



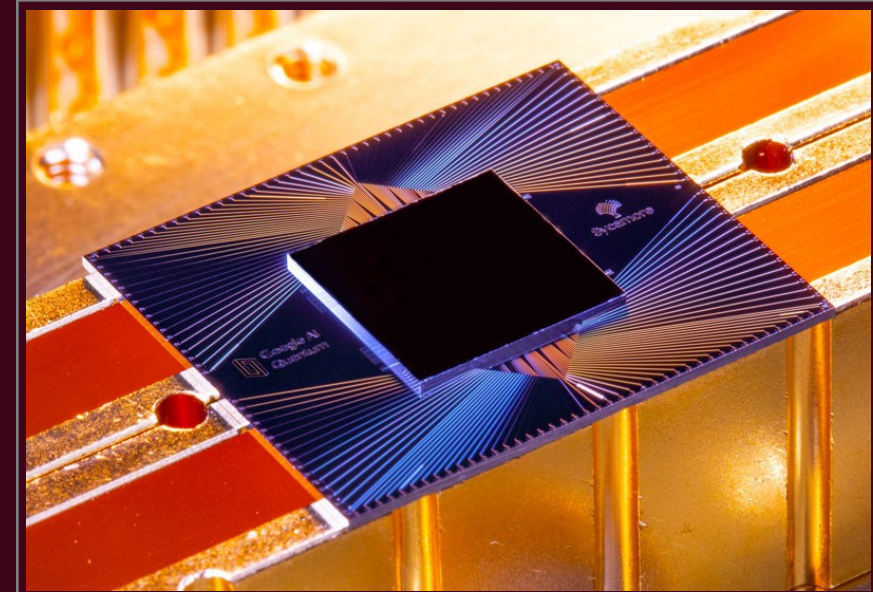
## Quantum Gate System

### Jaynes-Cummings Model

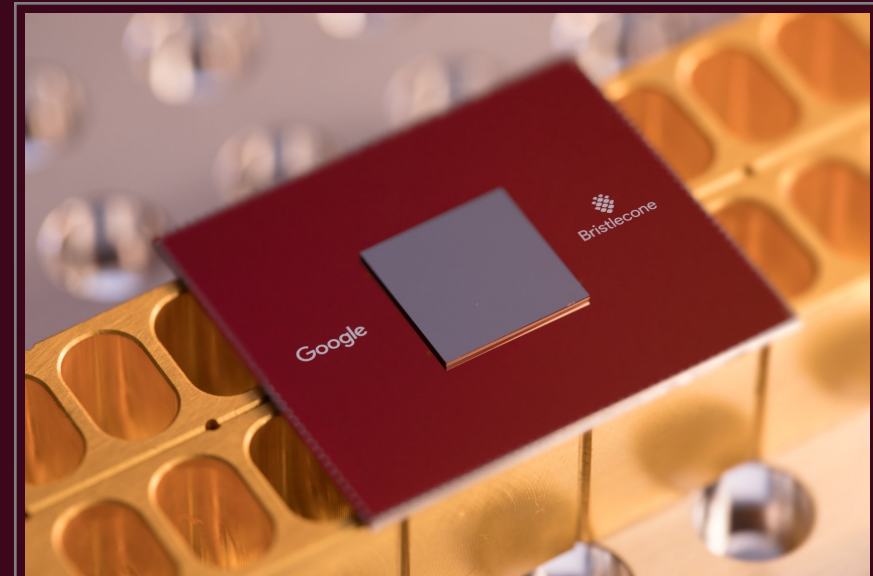
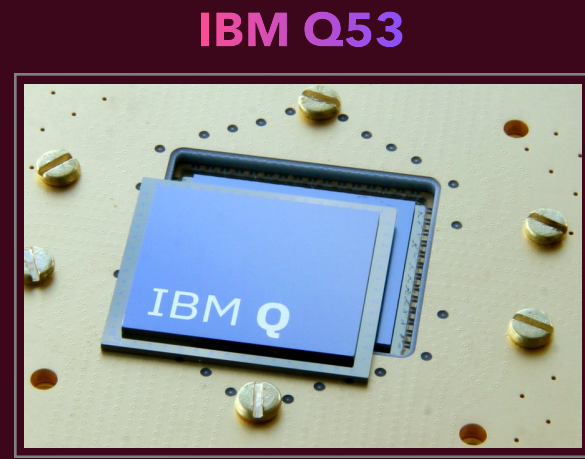
IBM 5-qubits



Google Sycamore 53-qubits



Google Bristlecone 72-qubits

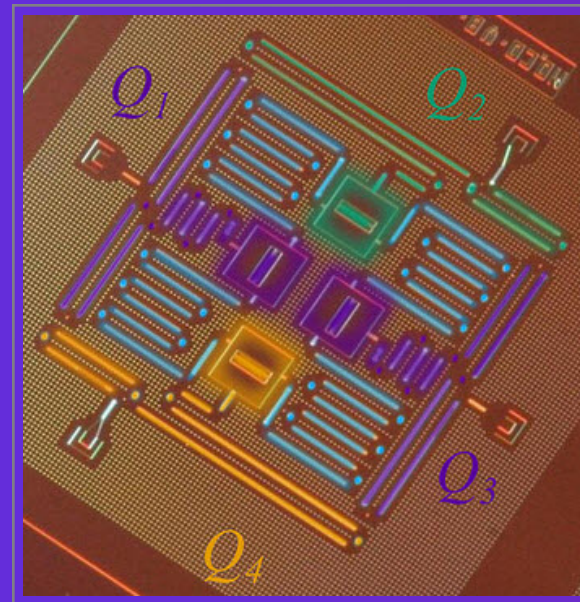


# GATE-BASED ARCHITECTURE

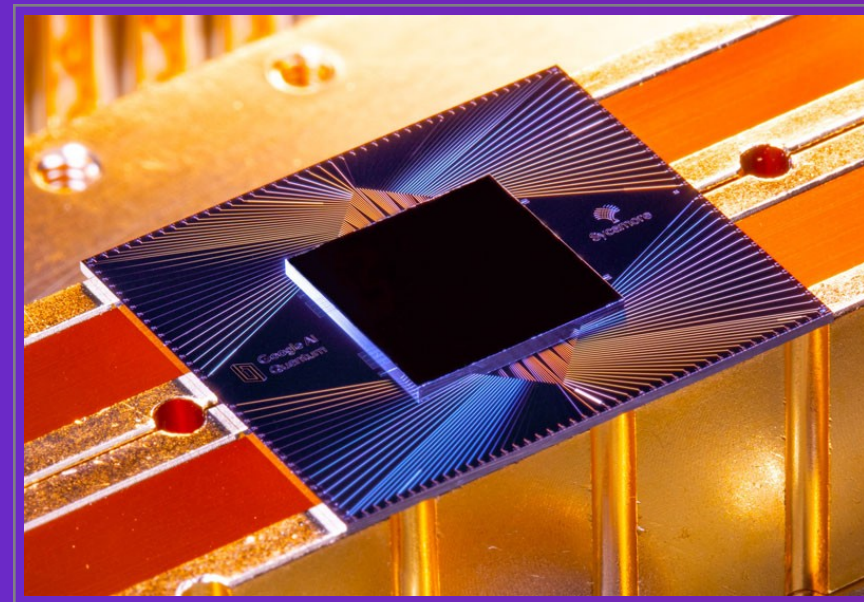
# MOTIVATION

Among the many proposed pristine quantum-bit platforms for quantum computing, the quantum gate-based superconducting circuit has become the leading candidate platform for large-scale quantum processor technology. Within this platform, the Josephson junction-based qubit (Jj-qubit) is today's core building block for state-of-the-art superconducting quantum processors, which is built in the same way as silicon chips.

IBM



Google



# PHYSICAL CONSTRAINTS

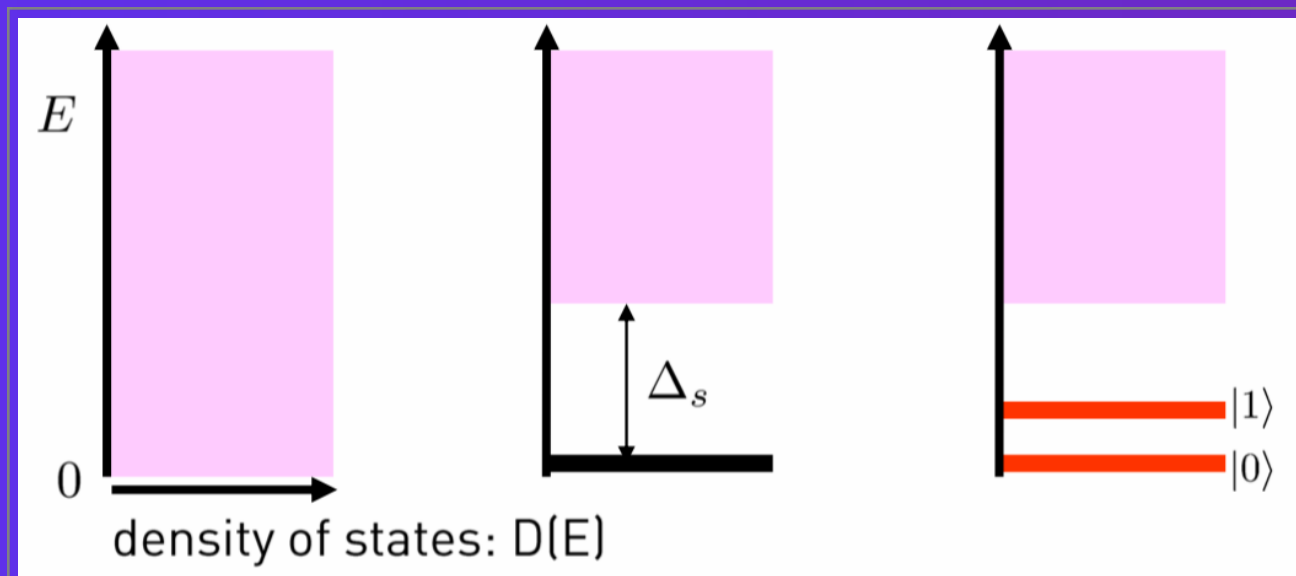
# CONSTRAINTS

**Aluminum (Al):**  $2\Delta_s/h = 100\text{GHz}$ ,  $T_c = 1.2K$

**Niobium (Nb):**  $2\Delta_s/h = 725\text{GHz}$ ,  $T_c = 9.2K$

$$T_c > 1K$$

**M. Tinkham.**



1. The thermal energy of the environment should be lower than the effective temperature of a photon in the resonator.

$$\kappa_b T \ll E = \hbar\omega_r \ll \Delta_s$$

2. The oscillator should be sufficiently well decoupled from uncontrolled degrees of freedom such that its energy levels are considerably less broad than their separation. In other words, we require the oscillator's quality factor to be large or, equivalently, to have long photon lifetime.

$$\kappa = \frac{\omega_r}{Q_L} = 10^3 \text{ to } 10^8$$

# STATE-OF-THE-ART

# BENCHMARKING GOOGLE'S BRITLEScone 72-QUBITS

**Joe Bardin et al., APS March Meeting 2020.**

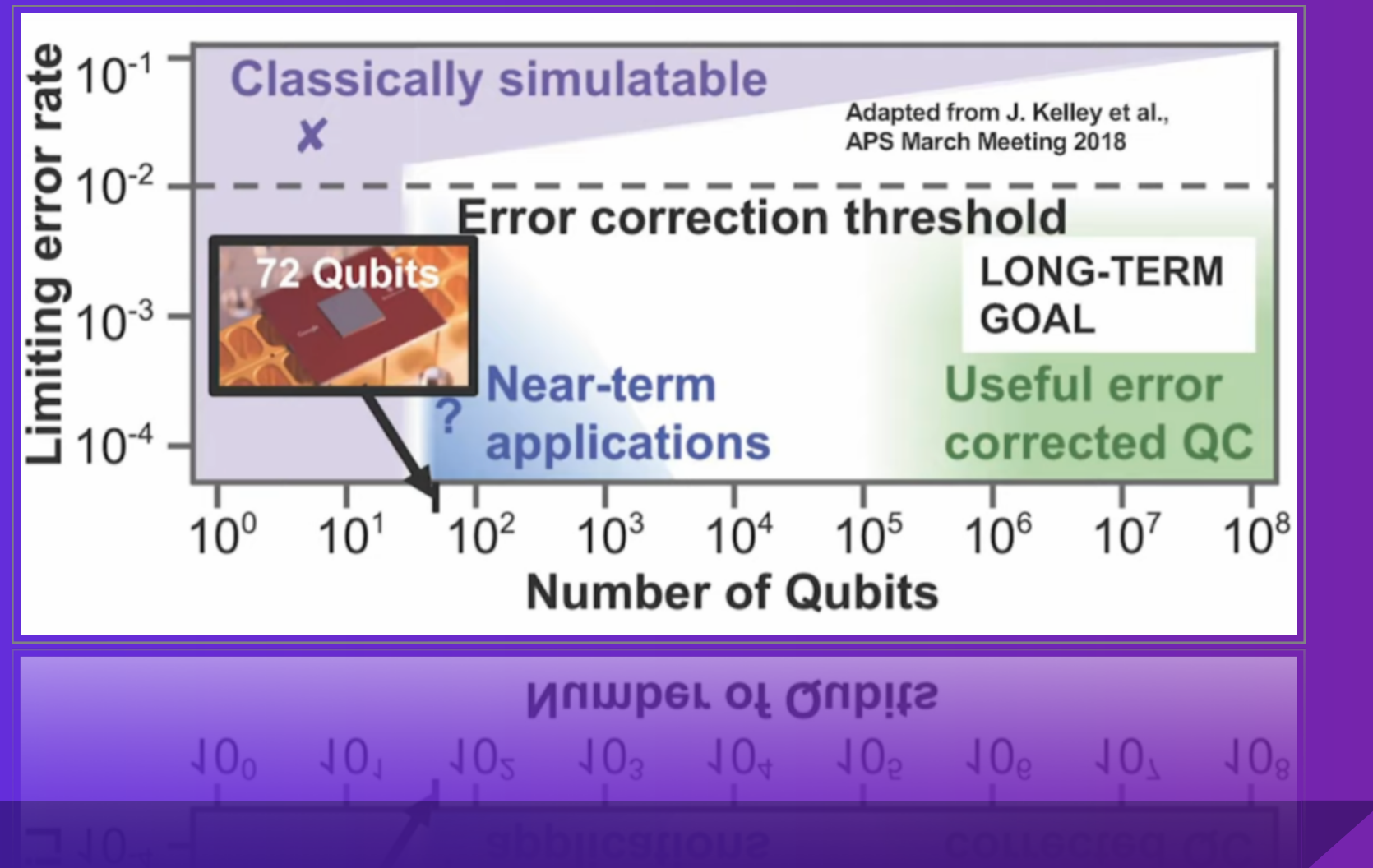


- 1. 240 High speed AWG (Arbitrary Waveform Generator): to shape the probe signal used for quantum gate operations;**
- 2. 84 Upconverters (DUC);**
- 3. 12 Downconverters (DDC);**
- 4. 24 High speed ADC (analog-to-digital converter): for readout of the qubit signal after amplification;**
- 5. 168 Long and lossy coax cables from 300K-to-4K: for signal transmission;**
- 6. 168 Superconducting coax cables (4K-to-10mK): at the lower temperature stages;**
- 7. Data stream of >3Tb/s.**

# MOTIVATION

## End game and practical applications

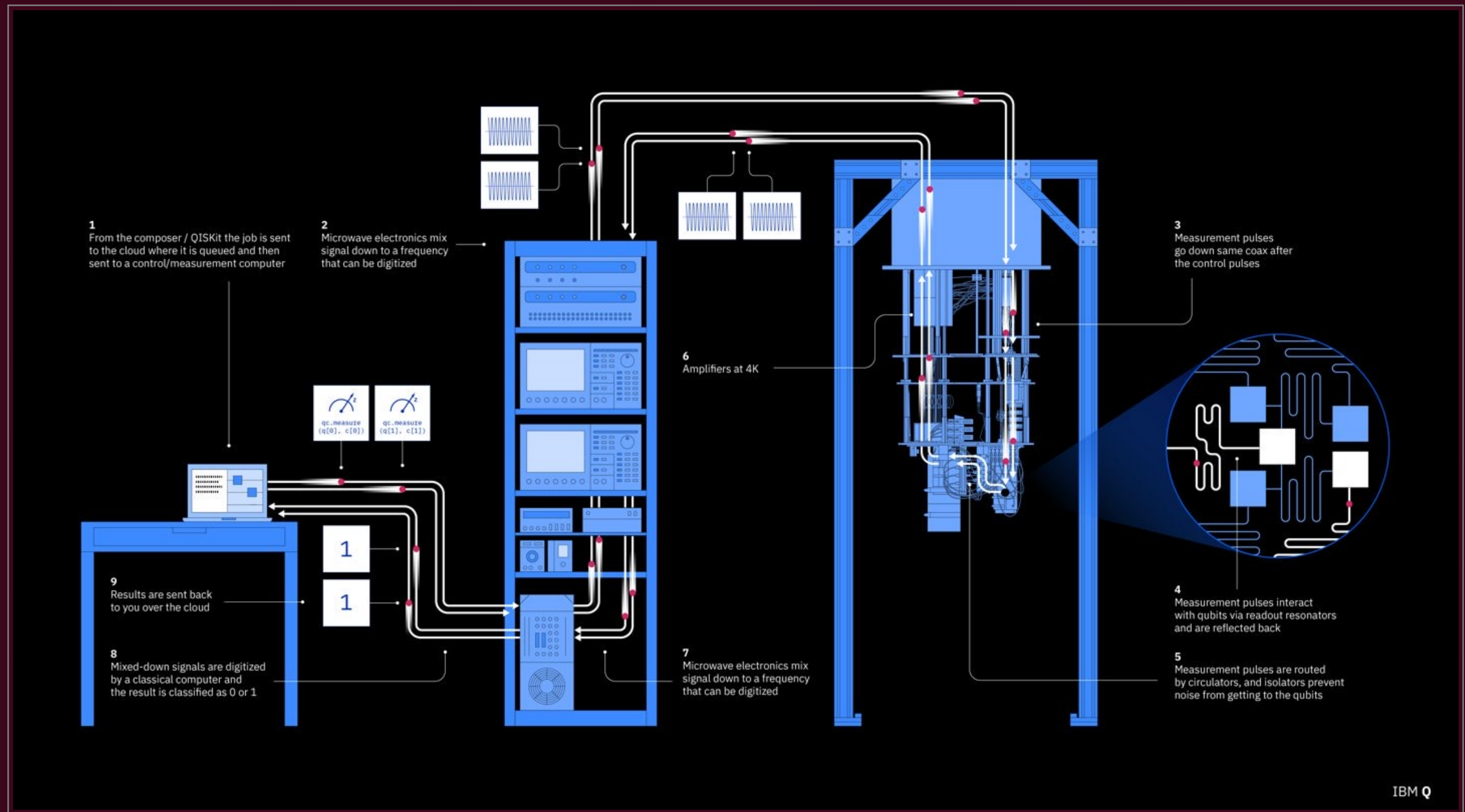
State-of-the-art (72 qubits) compared to practical quantum computing requirement of millions of qubits [Joe Bardin et al., APS March Meeting 2020]. Quantum error correction could solve the fundamental problem of decoherence, but it would require anywhere from 100 to 10,000 physical qubits per logical qubit.



# BLUEPRINT

# SUPERCONDUCTING QUANTUM COMPUTING BLUEPRINT

17

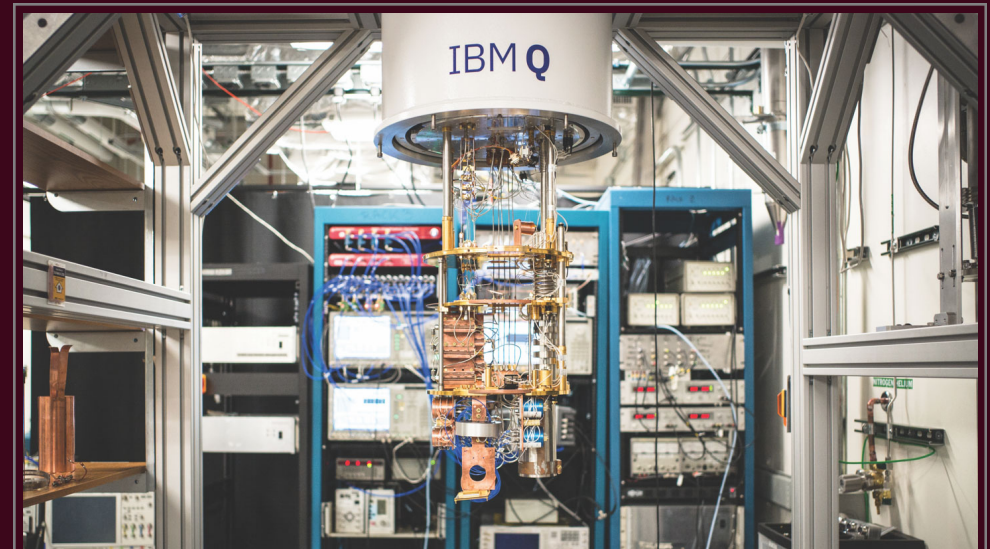
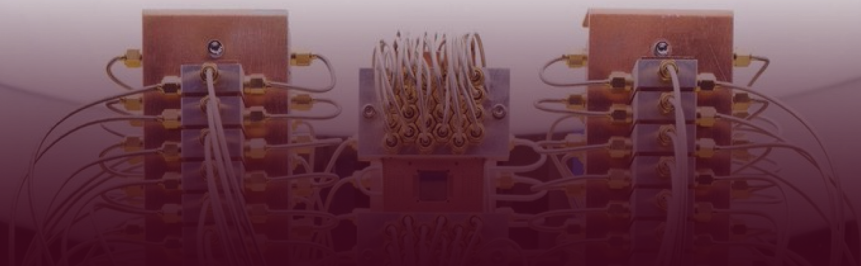
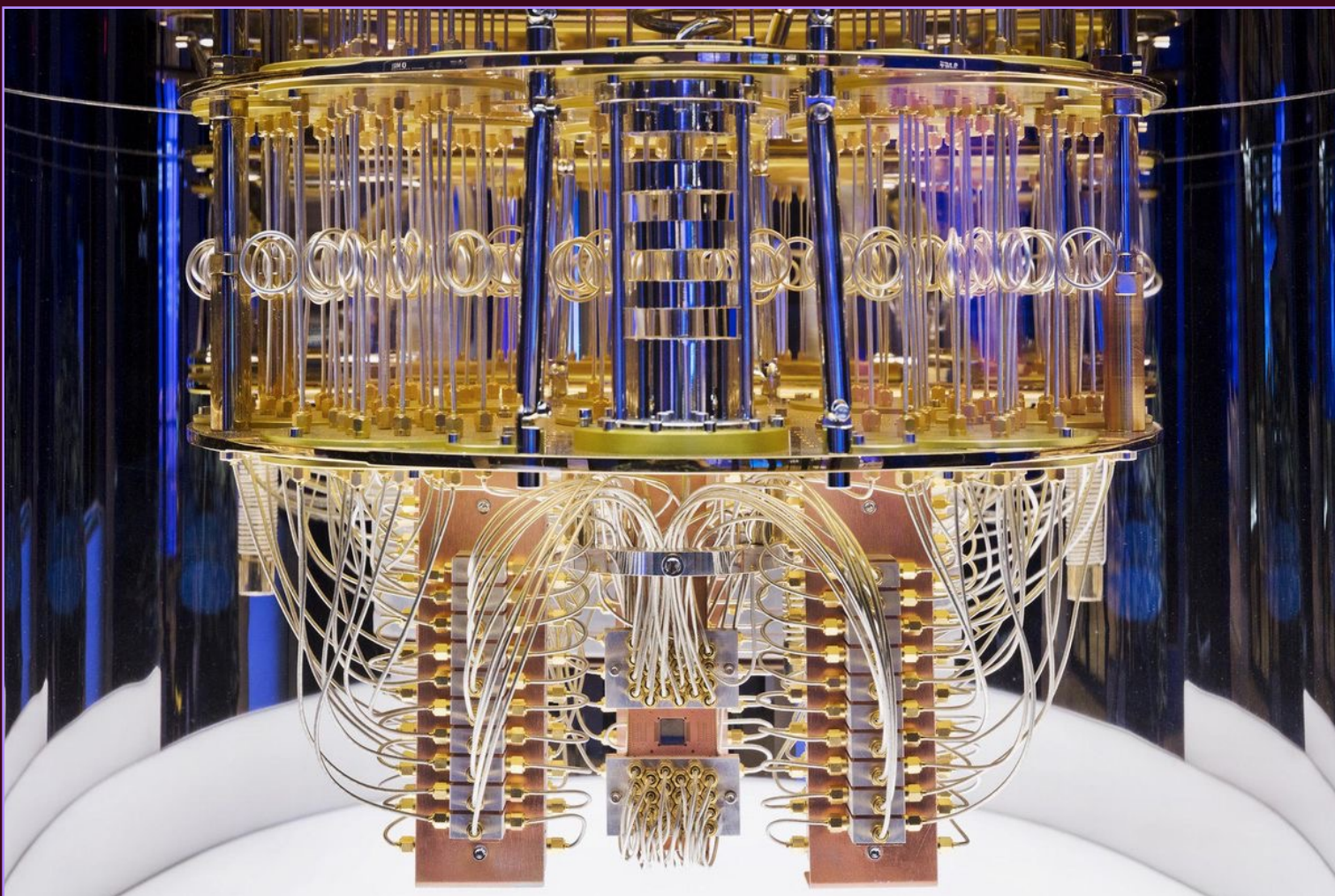


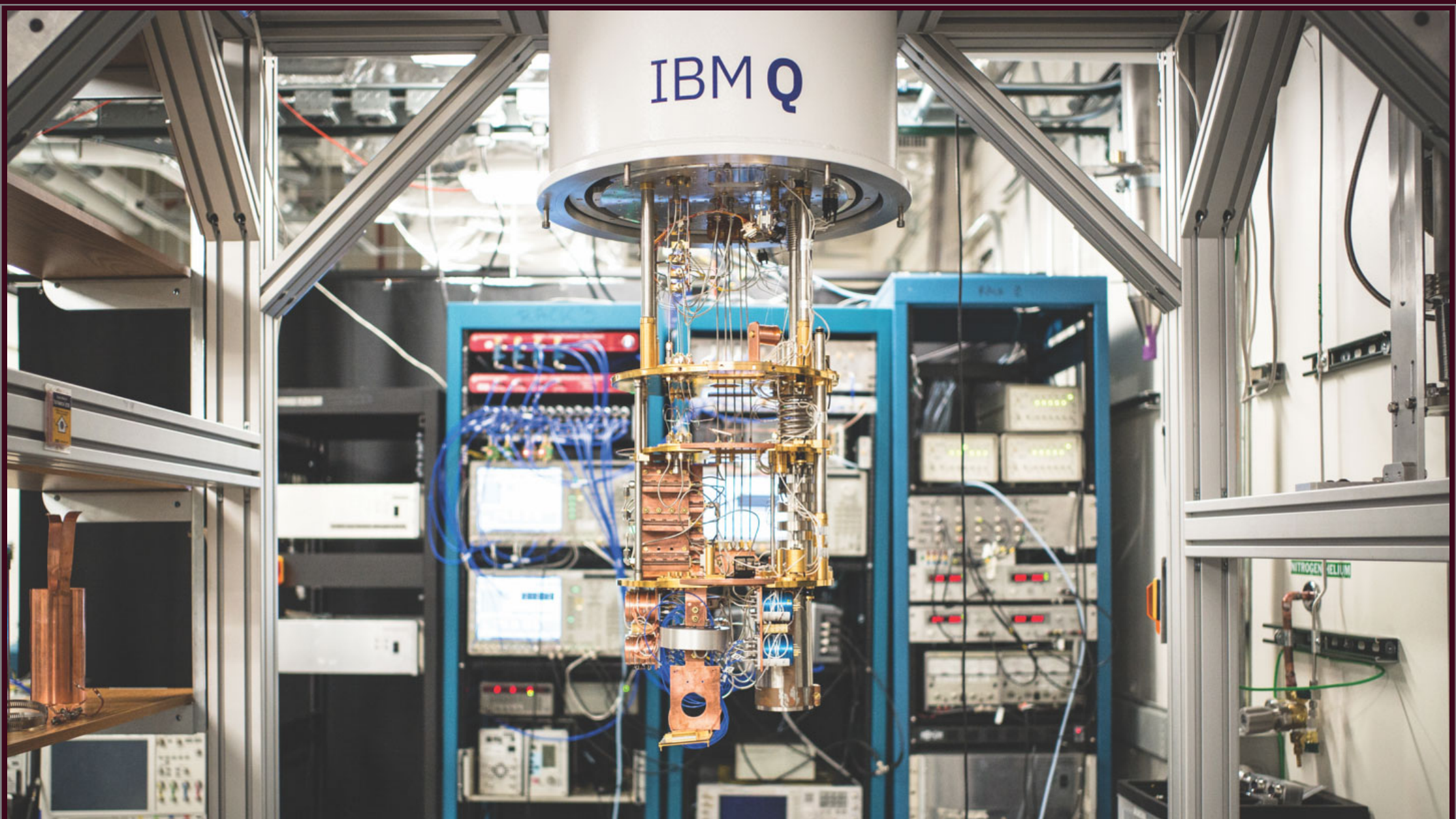
IBM Q

IBW Ø

Quantum computers are still big and noisy,  
reminding of the monolithic systems from the 1940s.

## IBM QUANTUM COMPUTER





## CRYPERM SHIELD



## Dry Dilution Refrigerator Cryostat: $^3\text{He}$ - $^4\text{He}$ mixture

### 1. Qubit Signal Amplifier:

One of two amplifying stages is cooled to a temperature of 4 Kelvin.

### 2. Input Microwave Lines

Attenuation is applied at each stage in the refrigerator in order to protect qubits from thermal noise during the process of sending control and readout signals to the processor.

### 3. Superconducting Coaxial Lines

In order to minimize energy loss, the coaxial lines that direct signals between the first and second amplifying stages are made out of superconductors.

### 4. Cryogenic Isolators

Cryogenic isolators enable qubits signals to go forward while preventing noise from compromising qubit quality.

### 5. Quantum Amplifiers

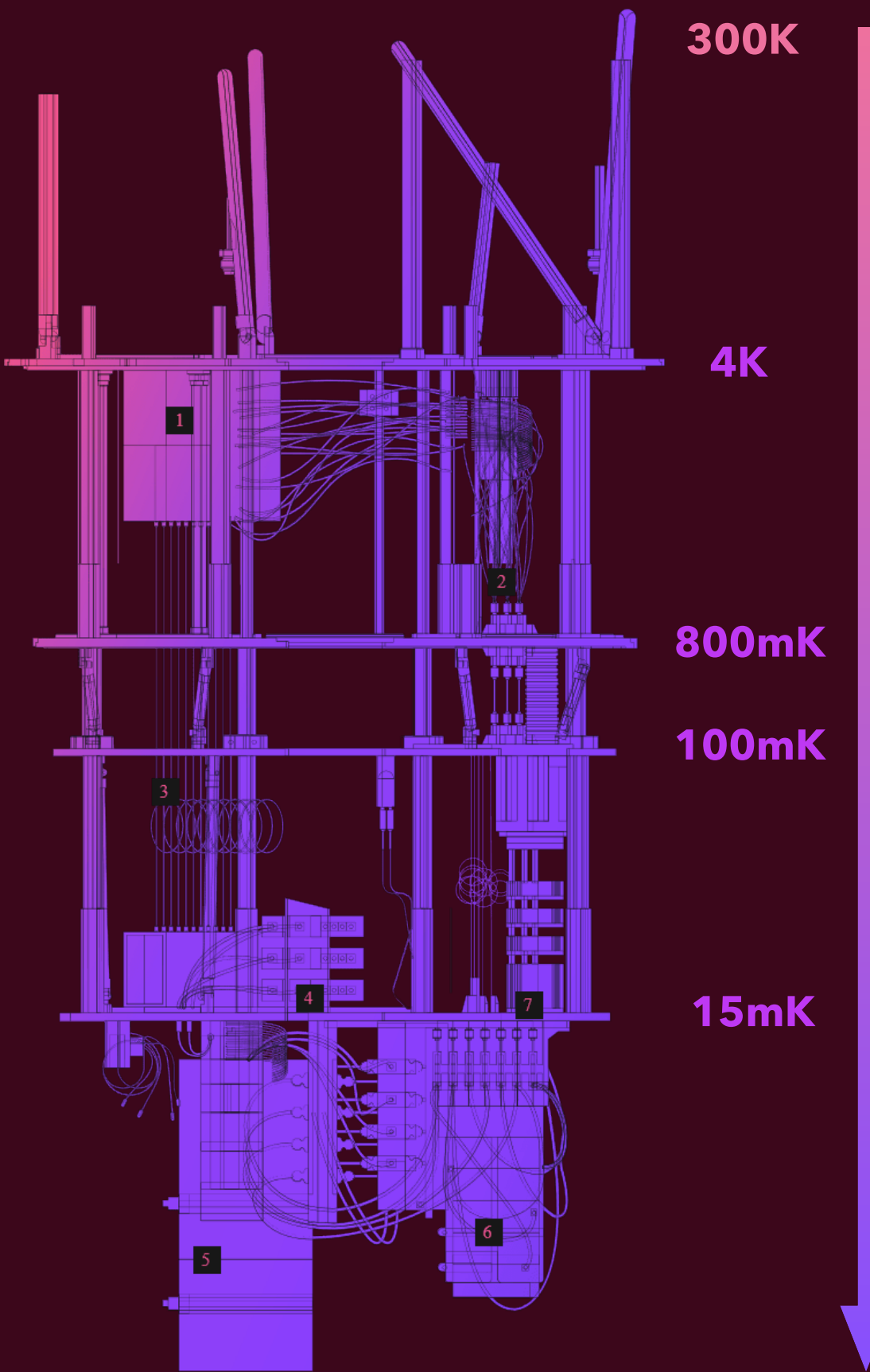
Quantum amplifiers inside of a magnetic shield capture and amplify processor readout signals while minimizing noise.

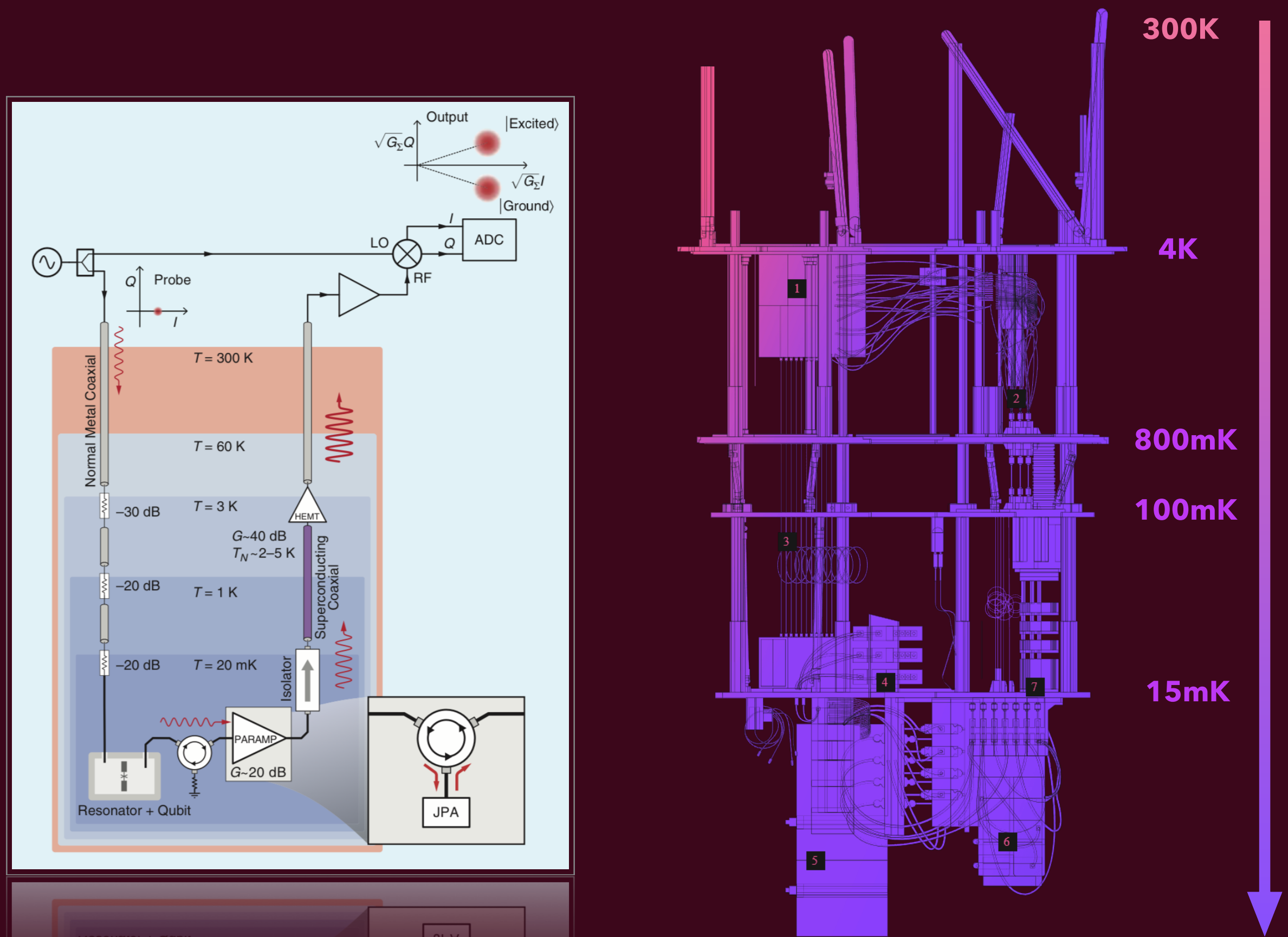
### 6. Cryoperm Shield

The quantum processor sits inside a shield that protects it from electromagnetic radiation in order to preserve its quality.

### 7. Mixing Chamber

The mixing chamber at the lowest part of the refrigerator provides the necessary cooling power to bring the processor and associated components down to a temperature of 15 mK – colder than outer space.





## MATERIALS - CABLES [1]

- › **High Temp. Coaxial wires (300K to 4K):**
  1. Gold SMPM cable connectors made from beryllium copper (BeCu) or brass with gold plating (up to 65 GHz);
  2. Copper or phosphor-bronze (PhBr) twisted pairs of diameters AWG35 and AWG36, respectively.

\*Gold does not rust, good thermal conductor (better than carbon metal); taunt metal cables can get snapped due to thermal dilation.
- › **Superconducting Coaxial wires (4K to 10mK):**  
 Alloy of Niobium-Titanium (Nb-Ti) -> Tc=10K.  
 \*Pure Gold is not a superconductor, it cannot form a cooper pair (two electrons) at cryogenic temperatures, i.e, it does not obey the Bardeen-Cooper-Schrieffer (BCS) theory.
- › **Superconducting Coplanar Waveguide Microwave Resonators**

Niobium (Nb) - Tc=9.26K.

Aluminium (Al) - Tc=1.2K.

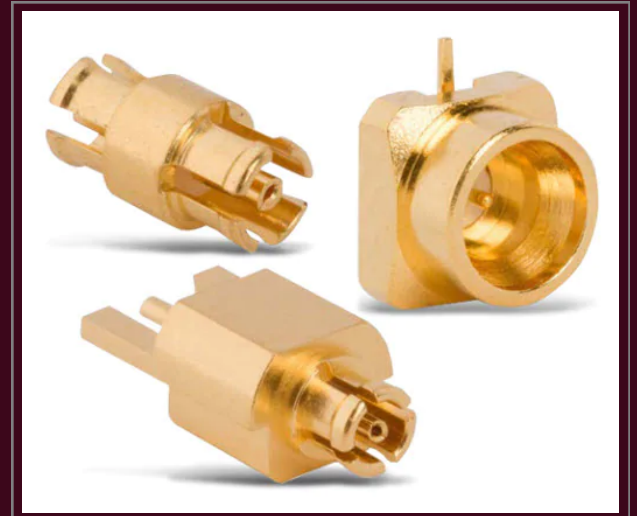
### SUPPLIERS:

AMPHENOL RF (HIGH TEMP.);

COAX CO. JAPAN (SUPERCONDUCTORS).

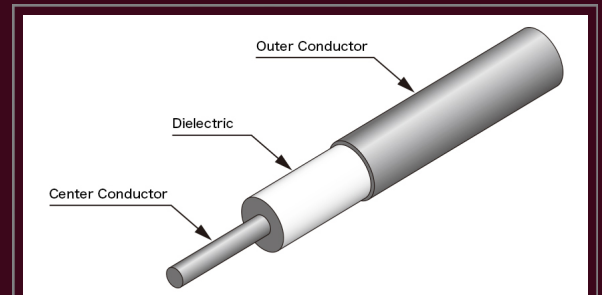
300K

SMPM Surface Mount PCB Jack, from Amphenol RF.  
Tmin=-65C (208.15 K).



4K

Niobium-titanium cable (UT-085-NbTi) from Coax Co.



10mK

# BUILDING BLOCKS

# CAPACITOR

**Current through a capacitor:**

$$I(t) = \frac{dQ_c}{dt} = \frac{d}{dt}(CV(t)) = C \frac{dV(t)}{dt},$$

**Stored kinetic energy:**

$$V = \frac{U}{q} \implies U = qV \implies dU = Vdq,$$

$$U_C = \int dU = \int_0^Q Vdq = \int_0^Q \frac{q}{c} dq = \frac{Q^2}{2C},$$

$$\begin{aligned} T_C(t) &= U_C(t) = \int_{-\infty}^t P(t')dt' = \int_{-\infty}^t I(t')V(t')dt', \\ &= \int_{-\infty}^t \left( C \frac{dV(t')}{dt'} \right) V(t')dt' = \frac{1}{2} CV(t)^2 = \frac{1}{2} C\dot{\Phi}^2. \end{aligned}$$

# INDUCTOR

**Voltage through an inductor:**

$$V(t) = -\dot{\Phi} = -\frac{d\Phi}{dt} = -\frac{d}{dt}(LI(t)) = -L \frac{dI(t)}{dt},$$

$$P(t) = \frac{dU(t)}{dt} = QV(t)/t = V(t)I(t),$$

**Stored potential energy:**

$$\begin{aligned} U_L(t) &= \int_{-\infty}^t P(t')dt' = \int_{-\infty}^t I(t')V(t')dt', \\ &= - \int_{-\infty}^t \left( L \frac{dI(t')}{dt'} \right) I(t')dt' = -\frac{1}{2}LI^2(t) = -\frac{1}{2}L\dot{Q}^2(t), \end{aligned}$$

$$\Phi(t) = \int_{-\infty}^t v_b(t')dt' = - \int_{-\infty}^t L \frac{dI(t')}{dt'}(t')dt' = -LI(t),$$

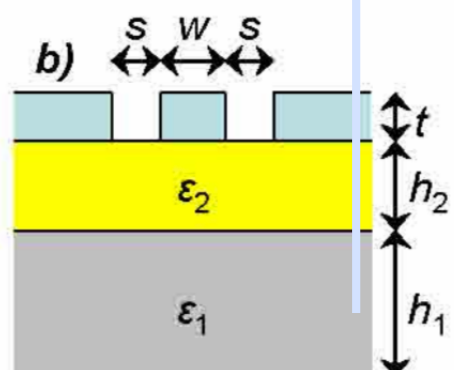
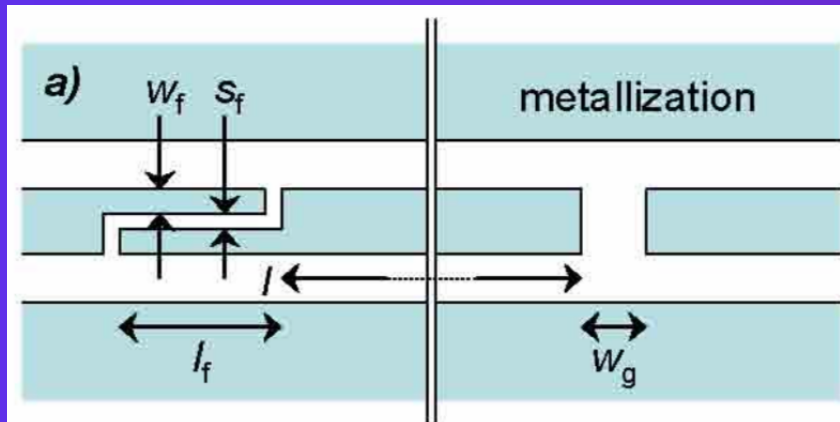
$$U_L(t) = -\frac{\Phi^2}{2L}.$$

# COPLANAR WAVEGUIDE (CPW)

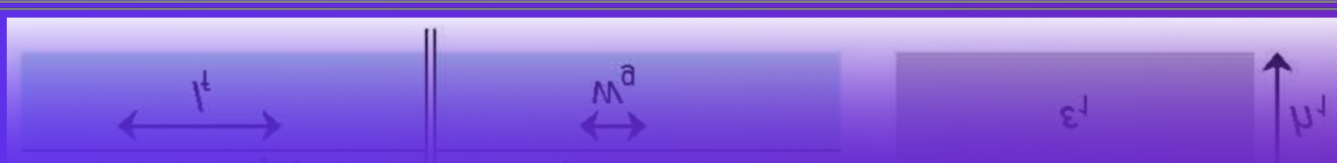
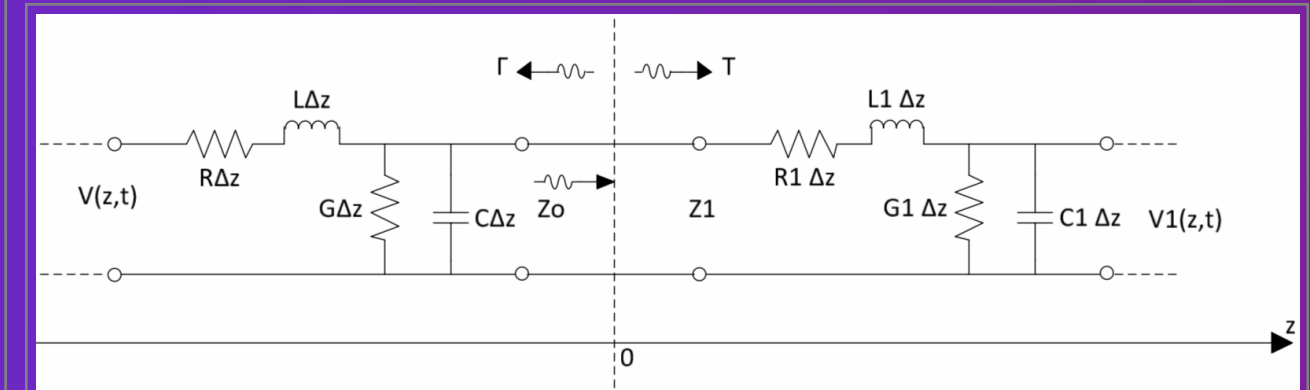
Lumped element model

$$\epsilon_r, \mu_r$$

M. Goppl et al. (2008).



Chalmes [Thesis]



# COPLANAR WAVEGUIDE (CPW)

## Propagation Modes of quasi-TEM

Part of the EM field fringes up to the free space, making the medium inhomogeneous thus requiring an effective permittivity.

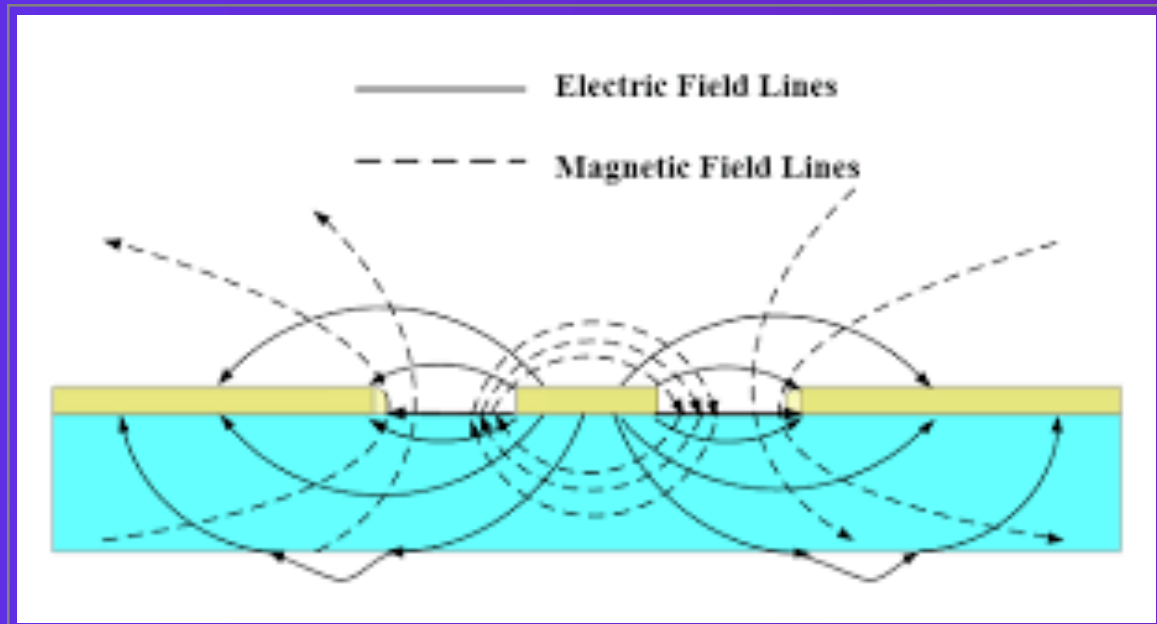
Conformal mapping technique

$$\epsilon_{eff} = \frac{1 + \epsilon_r K}{1 + K}$$

$$\epsilon_{eff} \approx \frac{\epsilon_{air} + \epsilon_r}{2} = \frac{1 + \epsilon_r}{2}$$

$$k_0 = \frac{w}{w + 2s} \quad k'_0 = \sqrt{1 - k_0^2}$$

$$\beta = \frac{2\pi}{\lambda_s} \sqrt{\epsilon_{eff}} \quad \lambda_0 = 2l$$



# COPLANAR WAVEGUIDE (CPW)

## Physical Parameters

Non-magnetic mat.:  $\mu_{eff} = 1$

c: velocity of light in vacuum;

Complete elliptic integral of the first kind;

Relative dielectric permitivity;

Effective dielectric permitivity;

Inductance per unit length;

Capacitance per unit length;

Characteristic impedance;

Phase velocity;

Resonator frequency;

Decay rate;

Quality factor;

**Zeroth-order quasi-static approximation**

$$\epsilon_{eff} = \frac{1 + \epsilon_r K}{1 + K} \approx \frac{1 + \epsilon_r}{2}$$

$$V_{ph} = \frac{1}{\sqrt{L_l C_l}} = c \sqrt{\frac{2}{1 + \epsilon_{eff}}}$$

$$L_l = \frac{L}{l} = \pm \frac{\mu_0}{4} \frac{K(k'_0)}{K(k_0)}$$

$$\omega_r = \frac{c}{\sqrt{\epsilon_{eff}}} \frac{1}{2l} = V_{ph} \frac{1}{2l}$$

$$C_l = \frac{C}{l} = 4\epsilon_0 \epsilon_{eff} \frac{K(k_0)}{K(k'_0)}$$

$$\kappa = \frac{\omega_r}{Q_L}$$

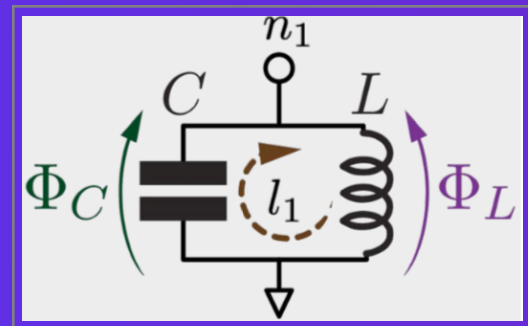
$$Z_0 = \sqrt{\frac{L_l}{C_l}} = \frac{1}{C_l V_{ph}}$$

$$V_{rms} = \sqrt{\frac{\hbar \omega_r}{l \cdot C_l}}$$

# RESONATOR

## Simple Harmonic Oscillator (SHO)

### Classical



$$\begin{aligned}\Phi &\rightarrow x \\ C &\rightarrow m \\ Q &\rightarrow p \\ L^{-1} &\rightarrow k\end{aligned}$$

$$\mathcal{L}(\Phi, \dot{\Phi}) = T - U = \frac{C\dot{\Phi}^2}{2} + \frac{\Phi^2}{2L},$$

$$H = q\dot{\Phi} - \mathcal{L} = \frac{Q^2}{2C} + \frac{\Phi^2}{2L}.$$

$$H = \frac{\hbar\omega_0}{2}(\hat{a}^*\hat{a} + \hat{a}\hat{a}^*)$$

$$\begin{aligned}\Phi &\rightarrow \hat{\Phi} \\ Q &\rightarrow \hat{Q}\end{aligned}$$

### Quantum

$$[\hat{\Phi}_n, \hat{Q}_n] = \hat{\Phi}_n \hat{Q}_n - \hat{Q}_n \hat{\Phi}_n = i\hbar$$

$$\hat{a} = \sqrt{\frac{1}{2\hbar Z_r}}(\hat{\Phi} + iZ_0\hat{Q}), \quad Z_r = \sqrt{\frac{L}{C}}$$

$$\hat{\Phi} = \Phi_{ZPF}(\hat{a}^\dagger + \hat{a}) = \sqrt{\frac{\hbar Z_r}{2}}(\hat{a}^\dagger + \hat{a}),$$

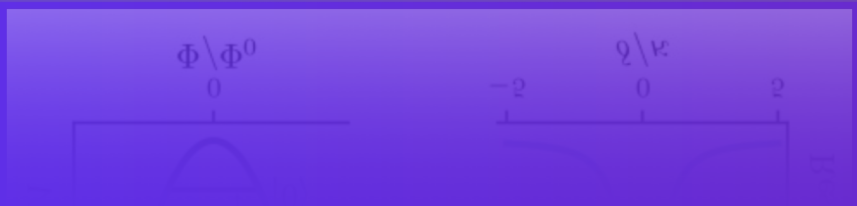
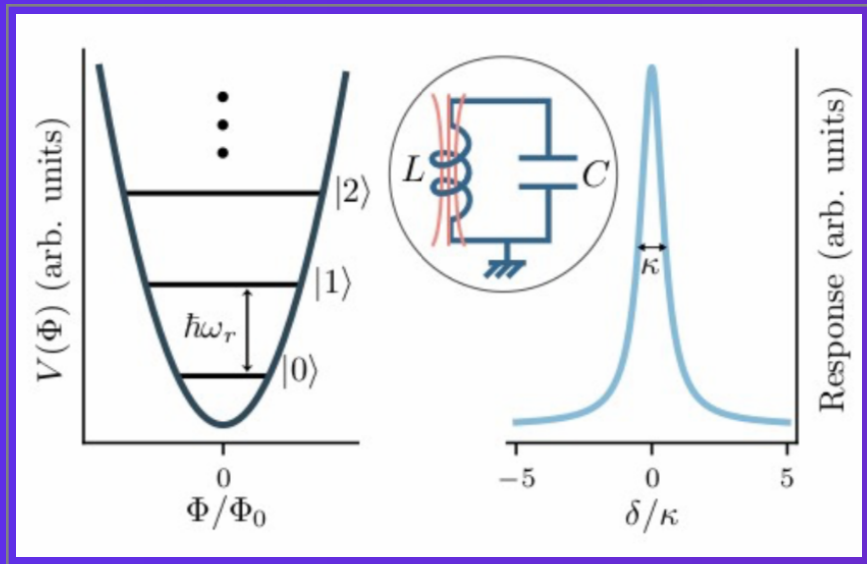
$$\hat{Q} = iQ_{ZPF}(\hat{a}^\dagger - \hat{a}) = i\sqrt{\frac{\hbar}{2Z_r}}(\hat{a}^\dagger - \hat{a}) = -i\sqrt{\frac{\hbar}{2Z_r}}(\hat{a} - \hat{a}^\dagger).$$

$$\hat{H} = \frac{\hbar\omega_r}{2}(\hat{a}^\dagger\hat{a} + \hat{a}\hat{a}^\dagger) = \hbar\omega_r(a^\dagger a + \frac{1}{2})$$

# RESONATOR

## Quantum harmonic oscillator

A. Blais et al. [Blais2020].



$\kappa$  ▶ Decay rate.

$$\kappa = \frac{\omega_r}{Q_L}$$

$\omega_r$  ▶ Resonator frequency.

$$\omega_r = \omega_{ij} = \sqrt{\frac{1}{LC}}$$

$$\hat{N} =: \hat{a}^\dagger \hat{a}$$

▶ Photon (Fock) number operator: indicates how many Fock states there is.

$$\hat{N}(\hat{N} - 1) |n\rangle = n(n - 1) |n\rangle$$

$|n\rangle$  ▶ Fock state: a.k.a energy eigenstate, indicates the number of photons (excitations) in a given energy level of the oscillator.

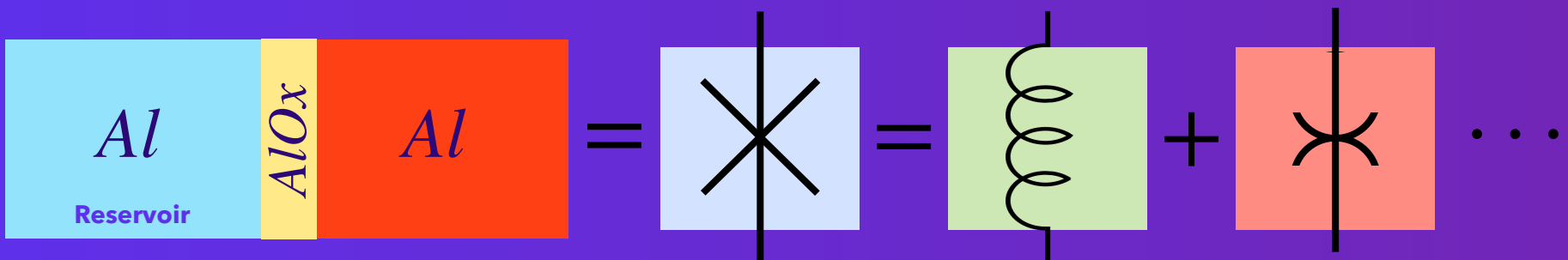
$$\hat{H} |n\rangle = \hbar\omega_r \left( n + \frac{1}{2} \right) |n\rangle$$

$$\hat{a} |n\rangle = \sqrt{n} |n-1\rangle$$

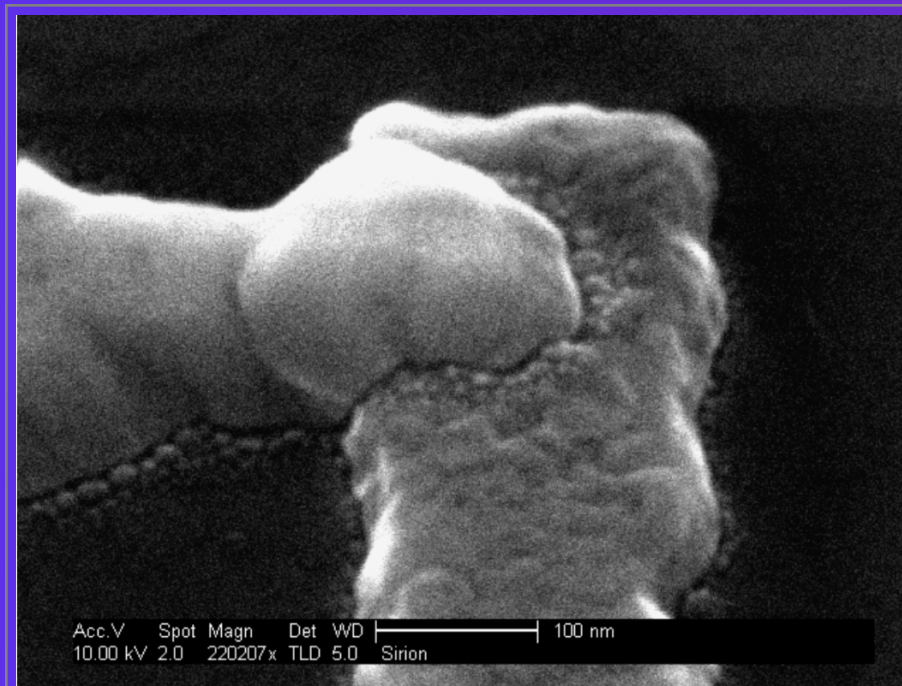
$$\hat{a}^\dagger |n\rangle = \sqrt{n+1} |n+1\rangle$$

# JOSEPHSON JUNCTION

The need for nonlinearity



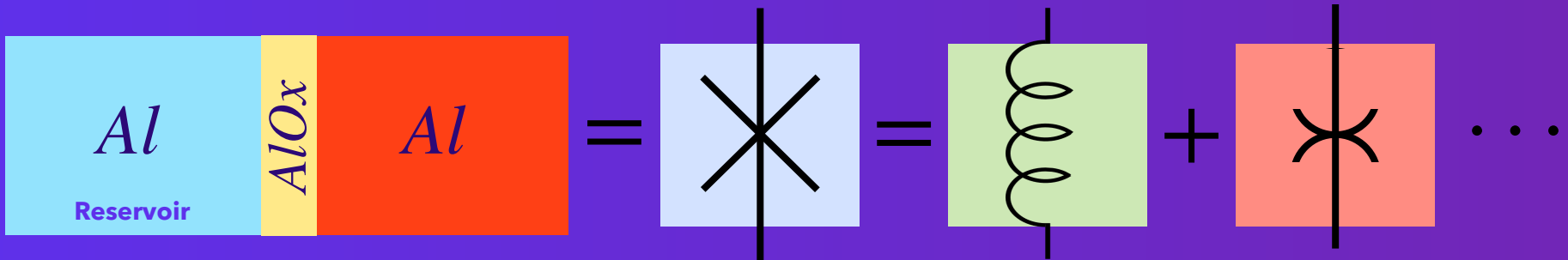
L. Frunzio.



**Across the entire chip everything  
is amorphous meaning that  
junctions will never grow the  
same and each will have a  
different physical parameter.**

# JOSEPHSON JUNCTION

The need for nonlinearity



Potential energy:

$$\begin{aligned}\epsilon_j(\Phi_j) &= E_j(1 - \cos(\Phi_j/\phi_0)) \\ &= \epsilon_j^{lin}(\Phi_j) + \epsilon_j^{nl}(\Phi_j) \\ &= \frac{E_j}{2!} \left( \frac{\Phi_j}{\phi_0} \right)^2 + \frac{E_j}{4!} \left( \frac{\Phi_j}{\phi_0} \right)^4 + \mathcal{O}(\Phi_j^6)\end{aligned}$$

$E_j$  ▶ Josephson energy required to tunnel one electron from the island to the reservoir.

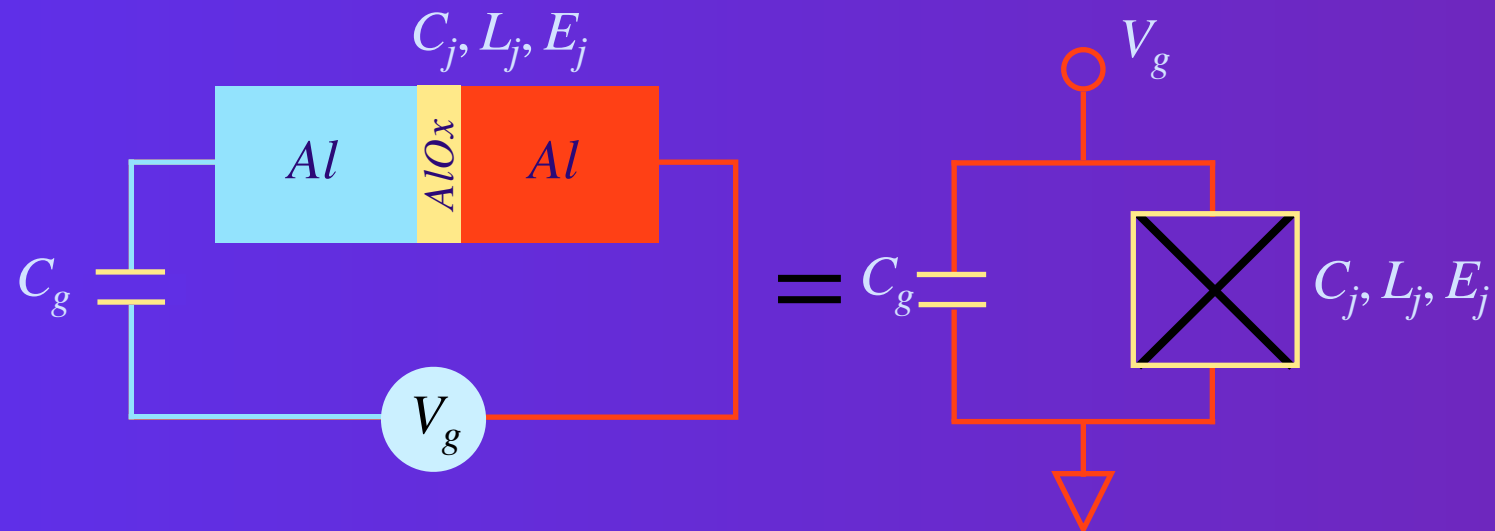
$$E_j = \frac{\phi_0^2}{L_j}$$

$\phi_0$  ▶ Flux quantum: the fundamental scale of flux as the cooper pair is for charge.

$$\phi_0 = \frac{\hbar}{2e} = 3.3 \times 10^{-16} \text{ Wb}$$

# COOPER-PAIR BOX

## Charge qubit



$$E_j/E_c \leq 1.$$

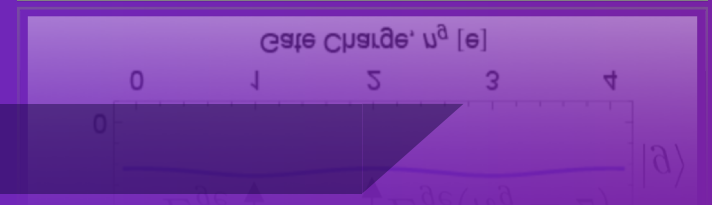
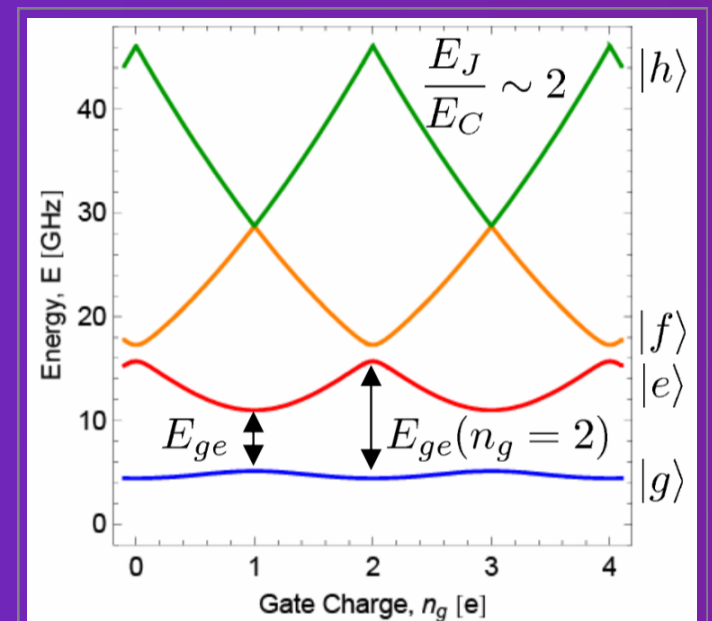
Controlled by a gate capacitance  $C_g$ .

Behaves like a charge qubit.

Drawbacks: charge noise.

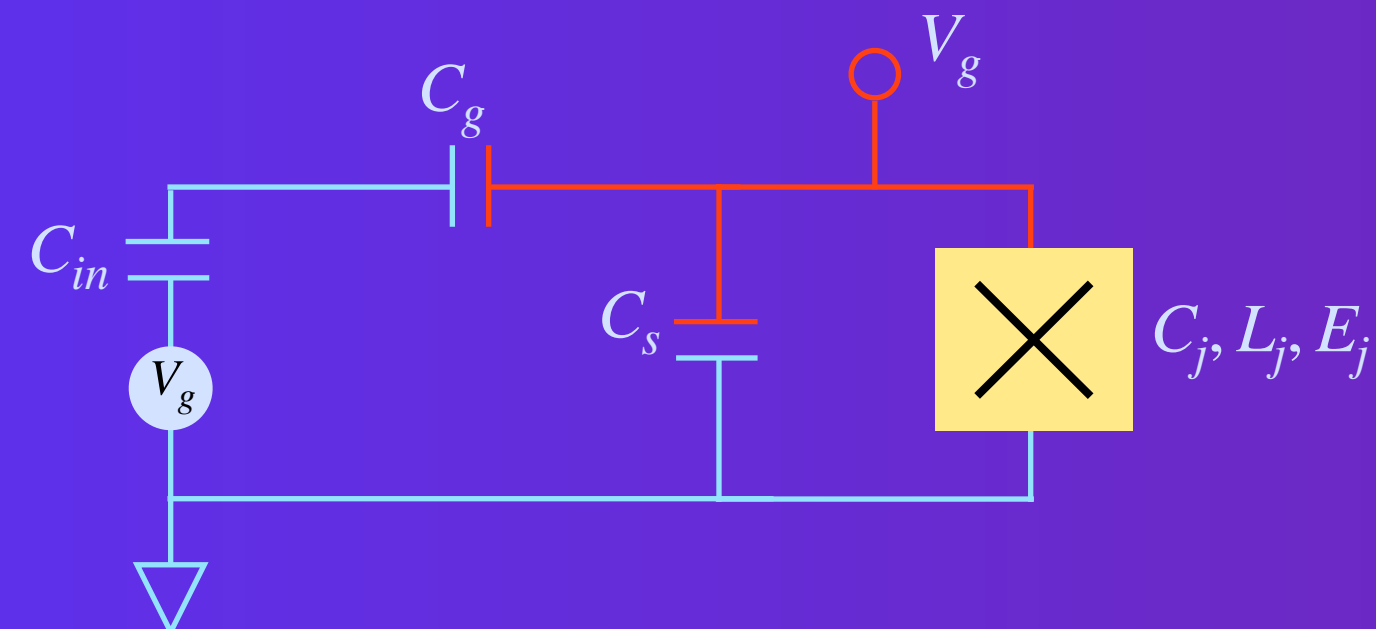
J. Koch et al. (Koch2007).

$$\begin{aligned} \hat{H} &= \frac{\hat{Q}^2}{2C_g} - E_j \cos(\hat{\Phi}/\phi_0) \approx \frac{\hat{Q}^2}{2C_g} + \frac{\hat{\Phi}^2}{2L_j} - \frac{E_j}{4!} \left( \frac{\Phi_j}{\phi_0} \right)^4 \\ &= \hbar\omega_0(\hat{a}^\dagger \hat{a}) - \frac{E_j \Phi_{ZPF}^4}{4!} (\hat{a} + \hat{a}^\dagger)^4 \end{aligned}$$

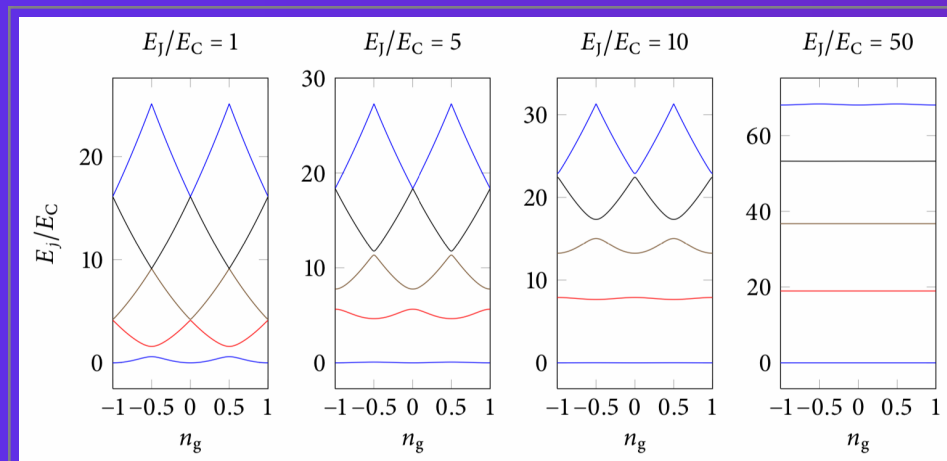


# TRANSMON QUBIT

## Charge qubit



Lev Bishop [Thesis2010]



$$E_j/E_c \gg 1.$$

Proposed by Koch et al. [Koch2007].

Controlled by a shunt capacitance:  $C_s$ .

Behaves like a charge qubit.

Advantages: charge noise can be suppressed.

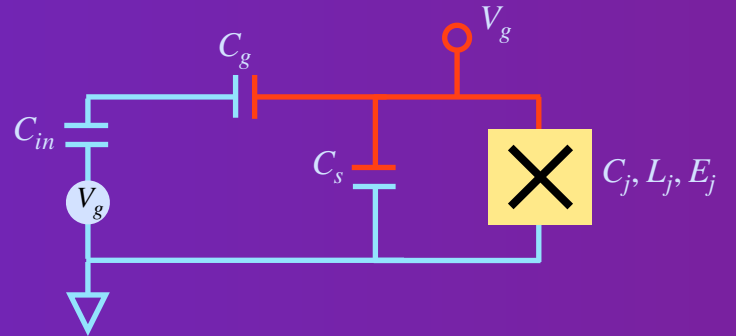
Drawbacks: fixed resonance frequency.

### Tradeoffs:

1. Smaller  $C$  gives more anharmonicity & enables faster gates.
2. The bigger the  $C$  value the smaller the charge dispersion.

# TRANSMON QUBIT

## Charge qubit



**Hamiltonian**

$$\begin{aligned}\hat{H} &= \frac{\hat{Q}^2}{2C_\Sigma} - E_j \cos(\hat{\Phi}/\phi_0) \\ &\approx \frac{\hat{Q}^2}{2C_\Sigma} + \frac{\hat{\Phi}^2}{2L_j} - \frac{E_j}{4!} \left( \frac{\Phi_j}{\phi_0} \right)^4 \\ &= \hbar\omega_0(\hat{a}^\dagger \hat{a}) - \frac{E_j \Phi_{ZPF}^4}{4!} (\hat{a} + \hat{a}^\dagger)^4\end{aligned}$$



**Rotating Wave Approximation (RWA)**

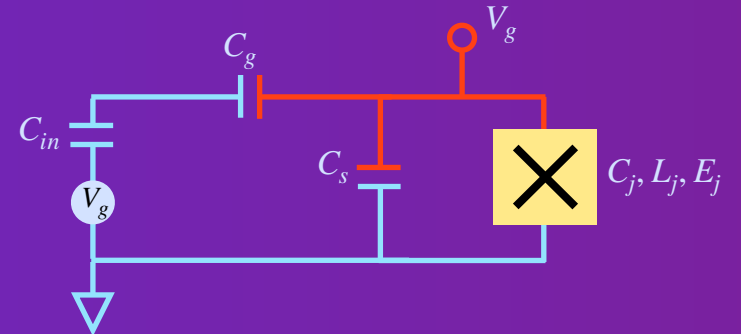
$$\hat{a}(t) = \hat{a}(0) = e^{-i\omega_0 t} \quad (\textbf{Heisenberg Picture})$$

$$\begin{aligned}\hat{H} &= \hbar\omega_0(\hat{a}^\dagger \hat{a}) - \frac{E_j \Phi^4}{4!} (12\hat{a}^\dagger \hat{a} + 6\hat{a}^{\dagger 2} \hat{a}^2) \\ &= \hbar(\omega_0 - \Delta_q) a^\dagger a - \frac{\hbar\alpha}{2} a^{\dagger 2} a^2\end{aligned}$$

$$\hat{H}_4^{RWA} \approx \hat{H}_{lin} + \hat{H}_{nl} = \hbar\omega_q \hat{N} - \frac{\hbar\alpha}{2} \hat{N}(\hat{N} - 1)$$

# TRANSMON QUBIT

## Charge qubit



$$\omega_0 = \sqrt{\frac{1}{LC}}$$

- **Bare frequency:** frequency of the linear part (SHO) of the qubit without the effect of the lamb shift.
- **Lamb shift:** is the energy difference between two energy levels, originally degenerated, that have been split apart in energy by a frequency  $\omega_0$ . The effect is the dressing of the qubit frequency by the nonlinearity due to vacuum energy fluctuations of the zero-point field (ZPF) which perturbs the potential energy landscape of the qubit.
- **Dressed/atomic transition frequency:** is the qubit frequency dressed by the nonlinearity due to zero-point vacuum fluctuations.

$$\begin{aligned}\alpha &=: \Delta_q = \frac{1}{2\hbar} E_j \Phi_{ZPF}^4 \\ &= \omega_0 - \omega_q\end{aligned}$$

$$\begin{aligned}\omega_q := \omega_{01} &= \omega_0 - \Delta_q = \frac{E_1 - E_0}{\hbar} \\ E_{01} &= hf = \hbar\omega_q\end{aligned}$$

# FLUX-TUNABLE TRANSMON

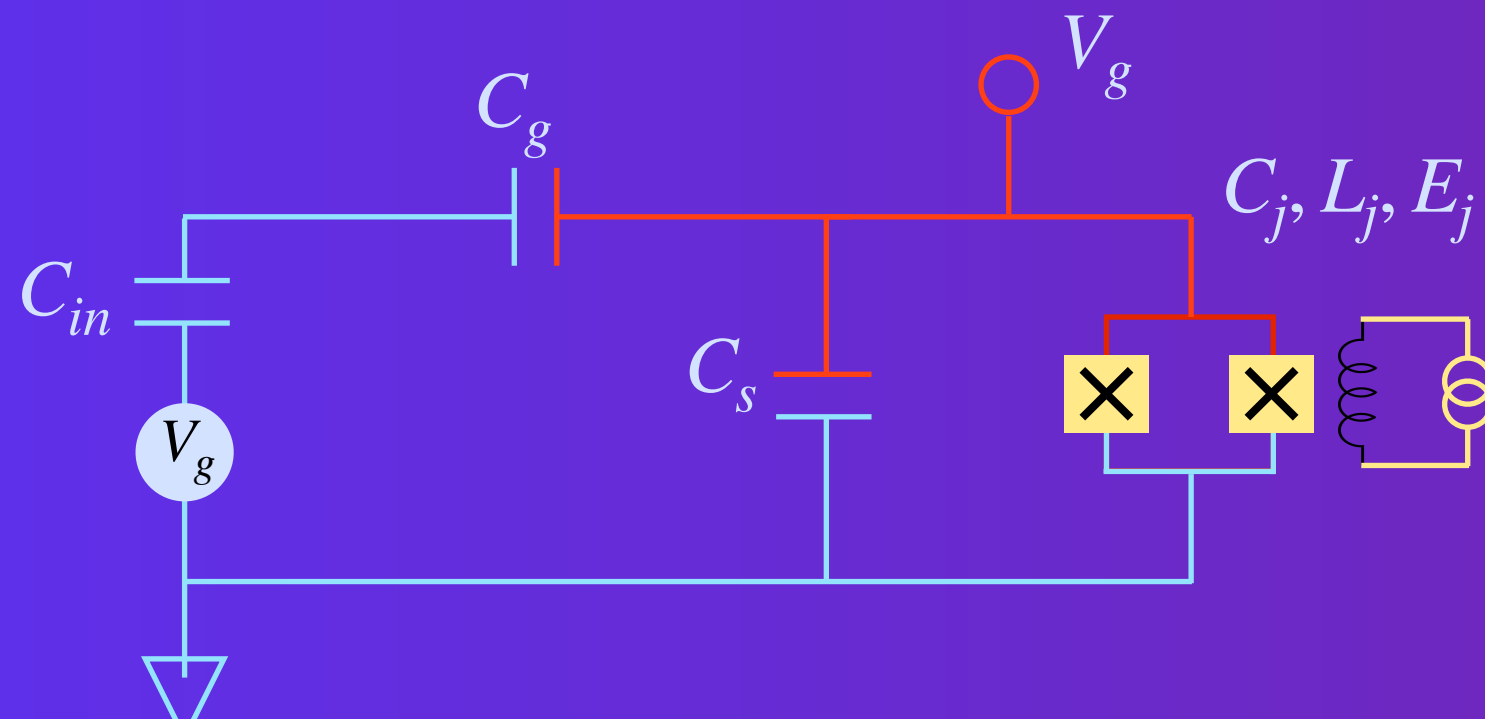
## Flux qubit

$$E_j/E_c > 1.$$

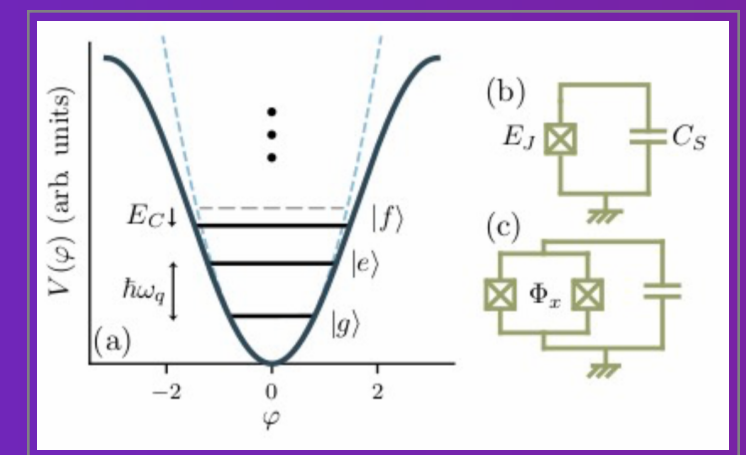
**Controlled by a shunt capacitance.**

**Behaves like a phase qubit.**

**Advantages: qubit frequency and resonator-qubit coupling tunability.**



A. Blais et al.

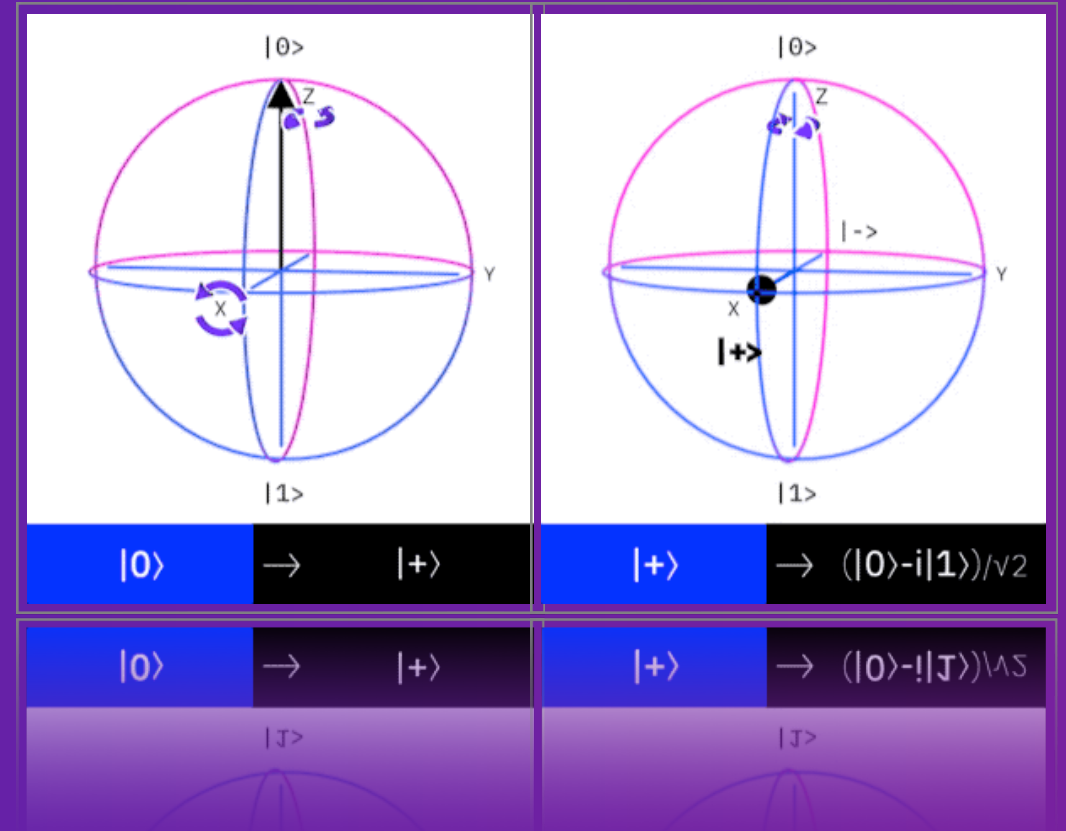
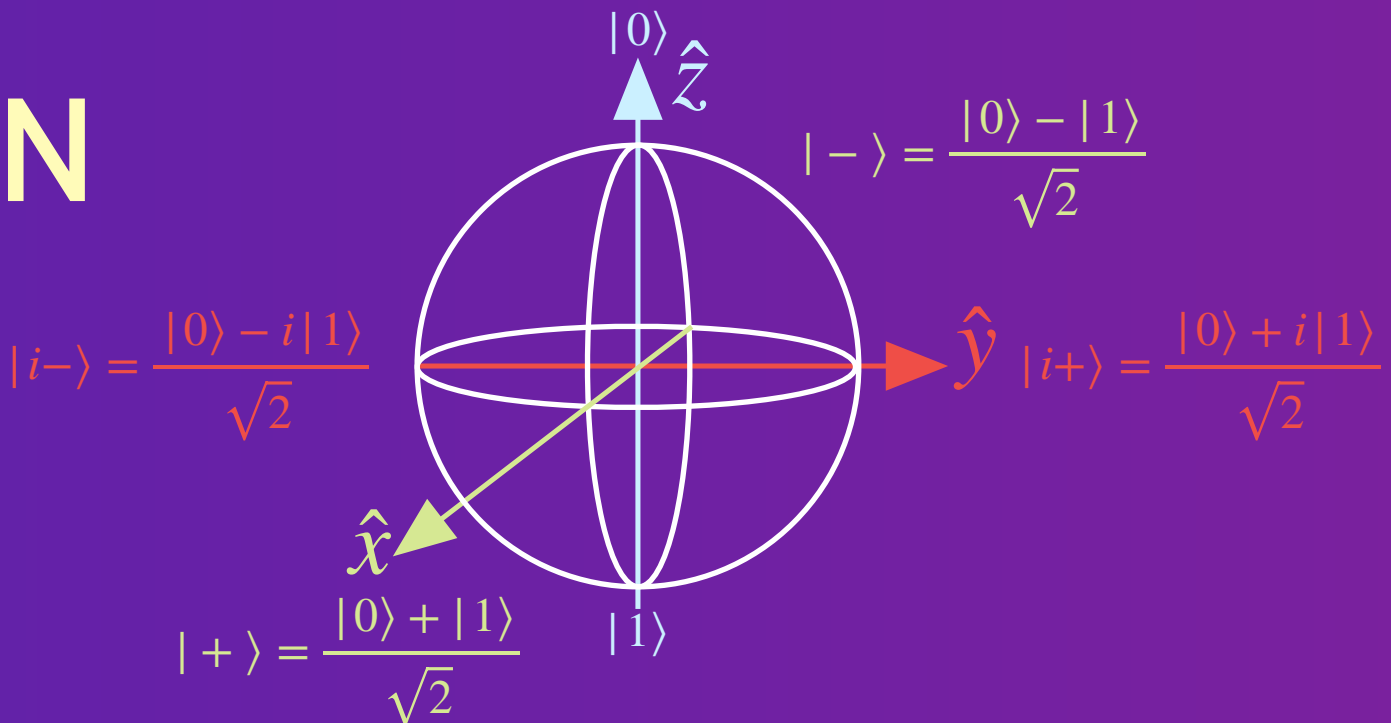


# GATE OPERATION

# MOTIVATION

1. Prepare superposition states;
2. Prepare entangled states;
3. Perform measurements.

$$|\psi\rangle = \frac{\cos(\theta/2)|0\rangle + e^{i\phi}\sin(\theta/2)|1\rangle}{\sqrt{2}}$$



# CLASSICAL-QUANTUM GATES

- Classical Computers

NAND

A	B	Output
0	0	1
0	1	1
1	0	1
1	1	0



$|0\rangle \otimes |1\rangle$

$= |0\rangle$

NOR

$= |1\rangle$

$|1\rangle$

$= |0\rangle$

$|0\rangle$

$= |1\rangle$

$|1\rangle$

$= |0\rangle$

- Quantum Computers

- Single-qubit rotations and a two-qubit operation such as

$|00\rangle = |0\rangle \otimes |0\rangle = \begin{pmatrix} 1 \\ 0 \\ 0 \\ 0 \end{pmatrix}$

cNOT

Input	Output
$ 00\rangle$	$ 00\rangle$
$ 01\rangle$	$ 01\rangle$
$ 10\rangle$	$ 10\rangle$
$ 11\rangle$	$ 10\rangle$



cPhase

Input	Output
$ 00\rangle$	$ 00\rangle$
$ 01\rangle$	$ 01\rangle$
$ 10\rangle$	$ 10\rangle$
$ 11\rangle$	$- 11\rangle$

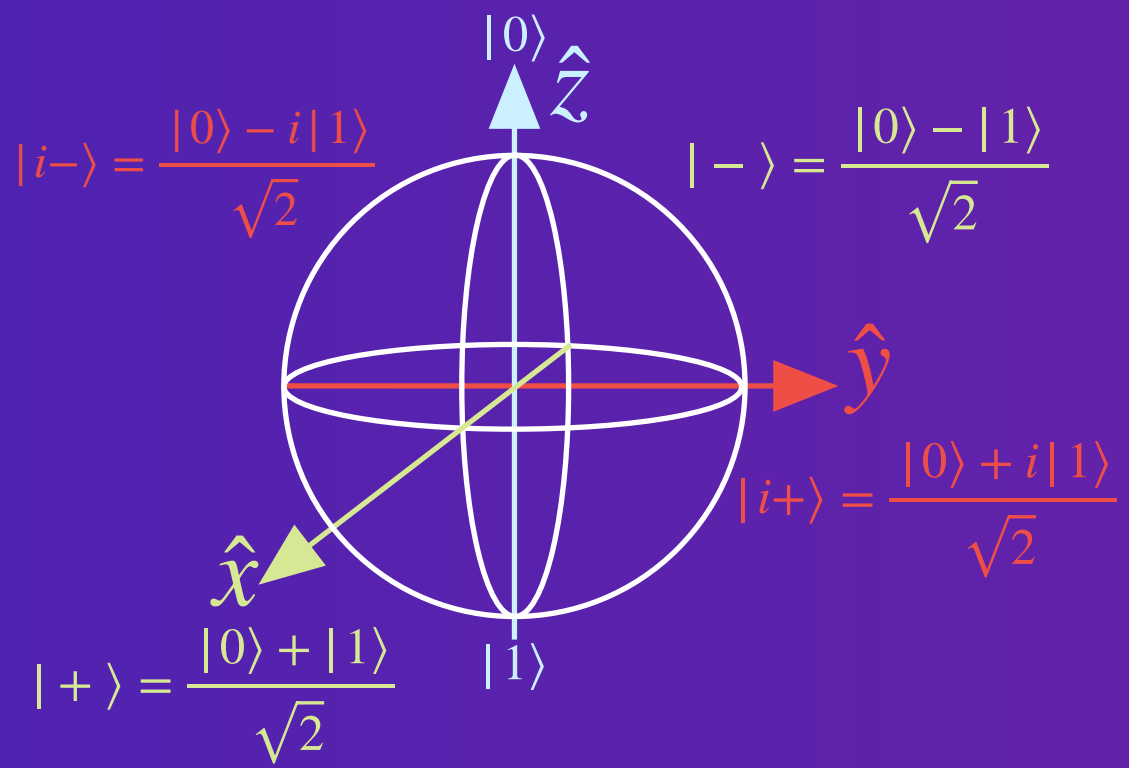


iSWAP

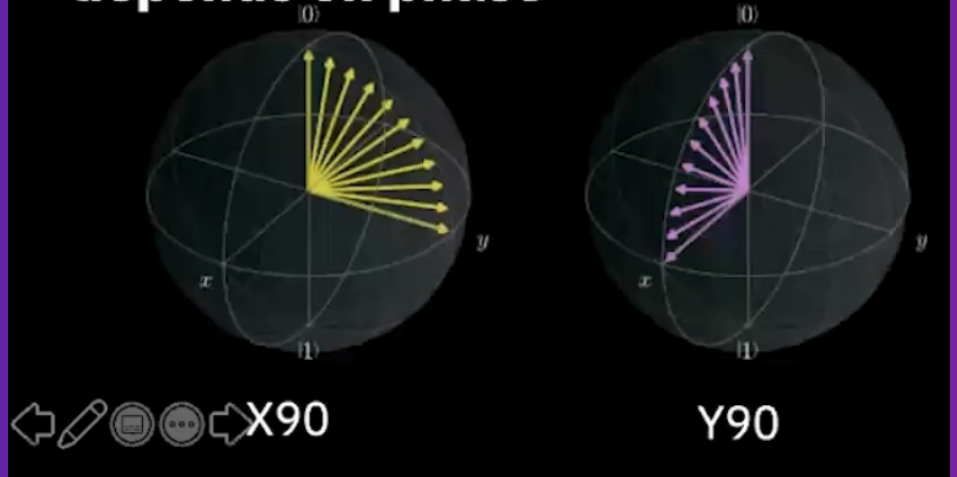
Input	Output
$ 00\rangle$	$ 00\rangle$
$ 01\rangle$	$i 10\rangle$
$ 10\rangle$	$i 01\rangle$
$ 11\rangle$	$ 11\rangle$



# BLOCH SPHERE



**Axis of rotation in Bloch sphere depends on phase**



- Computational States

$$|0\rangle = \begin{pmatrix} 1 \\ 0 \end{pmatrix} \quad |1\rangle = \begin{pmatrix} 0 \\ 1 \end{pmatrix}$$

- Pauli Matrices

$$X = \begin{pmatrix} 0 & 1 \\ 1 & 0 \end{pmatrix} \quad Y = \begin{pmatrix} 0 & -i \\ i & 0 \end{pmatrix} \quad Z = \begin{pmatrix} 1 & 0 \\ 0 & -1 \end{pmatrix}$$

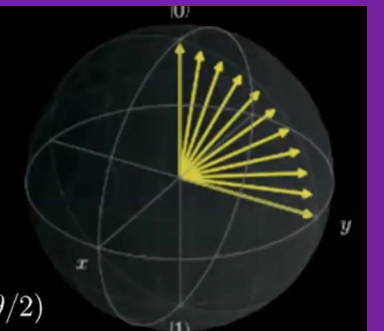
- Rotations around Bloch Sphere (gates)

$$R_{\hat{n}}(\theta) = \exp\{-i(\theta/2)\hat{n} \cdot \vec{\sigma}\} = \mathbf{I} \cos(\theta/2) - i(\hat{n} \cdot \vec{\sigma}) \sin(\theta/2)$$

$\mathbf{I}$  is identity matrix  $\vec{\sigma} = (X, Y, Z)$

- Example:  $\theta$  around  $x$ -axis

$$R_{\hat{x}}(\theta) = \begin{pmatrix} \cos(\theta/2) & -i \sin(\theta/2) \\ -i \sin(\theta/2) & \cos(\theta/2) \end{pmatrix}$$



X and Y are 90degree phase shifted

Gate	Circuit	Operation	Outcome $ \psi\rangle$
Pauli-X (NOT, Bit-flip)		$\begin{bmatrix} 0 & 1 \\ 1 & 0 \end{bmatrix} \begin{bmatrix} c_1 \\ c_2 \end{bmatrix}$	$c_1 1\rangle + c_2 0\rangle$
Pauli-Y (Y)		$\begin{bmatrix} 0 & -i \\ i & 0 \end{bmatrix} \begin{bmatrix} c_1 \\ c_2 \end{bmatrix}$	$i(c_1 1\rangle - c_2 0\rangle)$
Pauli-Z (Phase-flip)		$\begin{bmatrix} 1 & 0 \\ 0 & -1 \end{bmatrix} \begin{bmatrix} c_1 \\ c_2 \end{bmatrix}$	$c_1 0\rangle - c_2 1\rangle$
Hadamard (H, Superposition)		$\frac{1}{\sqrt{2}} \begin{bmatrix} 1 & 1 \\ 1 & -1 \end{bmatrix} \begin{bmatrix} c_1 \\ c_2 \end{bmatrix} \frac{(c_1 + c_2) 0\rangle + (c_1 - c_2) 1\rangle}{\sqrt{2}}$	
Phase (S, P)		$\begin{bmatrix} 1 & 0 \\ 0 & i \end{bmatrix} \begin{bmatrix} c_1 \\ c_2 \end{bmatrix}$	$c_1 0\rangle + ic_2 1\rangle$
$\pi/8$ (T)		$\begin{bmatrix} 1 & 0 \\ 0 & e^{i\pi/4} \end{bmatrix} \begin{bmatrix} c_1 \\ c_2 \end{bmatrix}$	$c_1 0\rangle + e^{i\pi/4}c_2 1\rangle$
Controlled NOT (cNOT, CX, Entanglement)		$\begin{bmatrix} 1 & 0 & 0 & 0 \\ 0 & 1 & 0 & 0 \\ 0 & 0 & 0 & 1 \\ 0 & 0 & 1 & 0 \end{bmatrix} \begin{bmatrix} c_1 \\ c_2 \\ c_3 \\ c_4 \end{bmatrix}$	$c_1 00\rangle + c_2 01\rangle + c_4 10\rangle + c_3 11\rangle$
Controlled Z (cPhase)		$\begin{bmatrix} 1 & 0 & 0 & 0 \\ 0 & 1 & 0 & 0 \\ 0 & 0 & 1 & 0 \\ 0 & 0 & 0 & -1 \end{bmatrix} \begin{bmatrix} c_1 \\ c_2 \\ c_3 \\ c_4 \end{bmatrix}$	$c_1 00\rangle + c_2 01\rangle + c_3 10\rangle - c_4 11\rangle$
SWAP		$\begin{bmatrix} 1 & 0 & 0 & 0 \\ 0 & 0 & 1 & 0 \\ 0 & 1 & 0 & 0 \\ 0 & 0 & 0 & 1 \end{bmatrix} \begin{bmatrix} c_1 \\ c_2 \\ c_3 \\ c_4 \end{bmatrix}$	$c_1 00\rangle + c_3 01\rangle + c_2 10\rangle + c_4 11\rangle$

Gate	Circuit	Operation	Outcome $ \psi\rangle$
Pauli-X (NOT, Bit-flip)		$\begin{bmatrix} 0 & 1 \\ 1 & 0 \end{bmatrix} \begin{bmatrix} c_1 \\ c_2 \end{bmatrix}$	$c_1 1\rangle + c_2 0\rangle$
Pauli-Y (Y)		$\begin{bmatrix} 0 & -i \\ i & 0 \end{bmatrix} \begin{bmatrix} c_1 \\ c_2 \end{bmatrix}$	$i(c_1 1\rangle - c_2 0\rangle)$
Pauli-Z (Phase-flip)		$\begin{bmatrix} 1 & 0 \\ 0 & -1 \end{bmatrix} \begin{bmatrix} c_1 \\ c_2 \end{bmatrix}$	$c_1 0\rangle - c_2 1\rangle$
Hadamard (H, Superposition)		$\frac{1}{\sqrt{2}} \begin{bmatrix} 1 & 1 \\ 1 & -1 \end{bmatrix} \begin{bmatrix} c_1 \\ c_2 \end{bmatrix} \frac{(c_1 + c_2) 0\rangle + (c_1 - c_2) 1\rangle}{\sqrt{2}}$	
Phase (S, P)		$\begin{bmatrix} 1 & 0 \\ 0 & i \end{bmatrix} \begin{bmatrix} c_1 \\ c_2 \end{bmatrix}$	$c_1 0\rangle + ic_2 1\rangle$
$\pi/8$ (T)		$\begin{bmatrix} 1 & 0 \\ 0 & e^{i\pi/4} \end{bmatrix} \begin{bmatrix} c_1 \\ c_2 \end{bmatrix}$	$c_1 0\rangle + e^{i\pi/4}c_2 1\rangle$
Controlled NOT (cNOT, CX, Entanglement)		$\begin{bmatrix} 1 & 0 & 0 & 0 \\ 0 & 1 & 0 & 0 \\ 0 & 0 & 0 & 1 \\ 0 & 0 & 1 & 0 \end{bmatrix} \begin{bmatrix} c_1 \\ c_2 \\ c_3 \\ c_4 \end{bmatrix}$	$c_1 00\rangle + c_2 01\rangle + c_4 10\rangle + c_3 11\rangle$
Controlled Z (cPhase)		$\begin{bmatrix} 1 & 0 & 0 & 0 \\ 0 & 1 & 0 & 0 \\ 0 & 0 & 1 & 0 \\ 0 & 0 & 0 & -1 \end{bmatrix} \begin{bmatrix} c_1 \\ c_2 \\ c_3 \\ c_4 \end{bmatrix}$	$c_1 00\rangle + c_2 01\rangle + c_3 10\rangle - c_4 11\rangle$
SWAP		$\begin{bmatrix} 1 & 0 & 0 & 0 \\ 0 & 0 & 1 & 0 \\ 0 & 1 & 0 & 0 \\ 0 & 0 & 0 & 1 \end{bmatrix} \begin{bmatrix} c_1 \\ c_2 \\ c_3 \\ c_4 \end{bmatrix}$	$c_1 00\rangle + c_3 01\rangle + c_2 10\rangle + c_4 11\rangle$

# DRIVE HAMILTONIAN

# DRIVE HAMILTONIAN

- **Drive Hamiltonian:**

$$V_D(t) = E_0 \cos(\omega_{01} t)$$

$$\hat{H}_D(t) = \frac{\hbar}{2} \omega_q (-\hat{\sigma}_z) + V_D(t) Q_{ZPF} \frac{C_D}{C} \hat{\sigma}_y$$

$$Q_{ZPF} = \sqrt{\frac{\hbar}{2Z}}$$

$$Z = \frac{L_\Phi}{C}$$

- **Driven Rotating Wave Approximation (RWA):**

$$\omega_q = \frac{1}{L_\Phi C}$$

$$\hat{H}_{RWA,D}(t) = \frac{e(t)}{2} Q_{ZPF} \left( \cos(\Phi_D) \hat{\sigma}_x + \sin(\Phi_D) \hat{\sigma}_y \right)$$

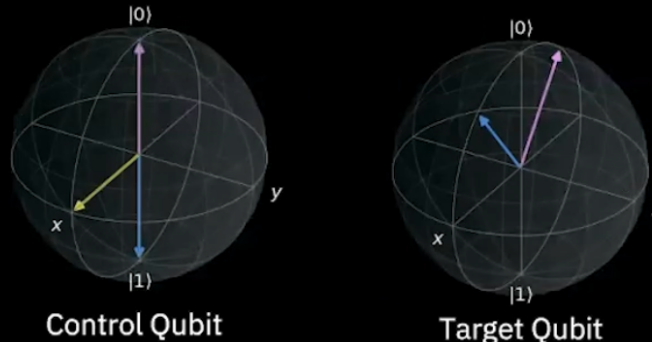
# DRIVE HAMILTONIAN

- **The microwave pulse have a gaussian shape with a carrier frequency at the transition frequency of the qubit. Then we put a derivative component on the quadrature (a.k.a drag pulse) for removal of the adiabatic gate which helps prevent leakage to the two state.**

**Axis of rotation in Bloch sphere depends on phase.**

$$\hat{H}_D(t) = \frac{\hbar}{2}\omega_q(-\hat{\sigma}_z) + V_D(t)Q_{ZPF} \frac{C_D}{C} \hat{\sigma}_y$$

- Cross Resonance: ZX Operation
- Rotation of Target Qubit depends on state of Control Qubit



$$ZX = Z \otimes X = \begin{pmatrix} 1 & 0 \\ 0 & -1 \end{pmatrix} \otimes \begin{pmatrix} 0 & 1 \\ 1 & 0 \end{pmatrix} = \begin{pmatrix} 0 & 1 & 0 & 0 \\ 1 & 0 & 0 & 0 \\ 0 & 0 & 0 & -1 \\ 0 & 0 & -1 & 0 \end{pmatrix}$$

$$U_{\text{CR}}(\theta) = \exp\{-i(\theta/2)ZX\} = \begin{pmatrix} \cos(\theta/2) & -i\sin(\theta/2) & 0 & 0 \\ -i\sin(\theta/2) & \cos(\theta/2) & 0 & 0 \\ 0 & 0 & \cos(\theta/2) & i\sin(\theta/2) \\ 0 & 0 & i\sin(\theta/2) & \cos(\theta/2) \end{pmatrix}$$

dotted line is the condition where there's no bus coupling between the qubits. as soon as they are coupled the qubits get hybridized in such a way that the 10 and 01 states will shift away in energy by an amount  $j^2/2\Delta$ . Where delta is the detuning in frequency of the two qubits

## Two Qubit Control: Cross Resonance

IBM Quantum

- Cross resonance is an all-microwave entangling gate
- Static  $J$ -coupling hybridizes the qubit levels
- Drive the control qubit at the target qubit's frequency

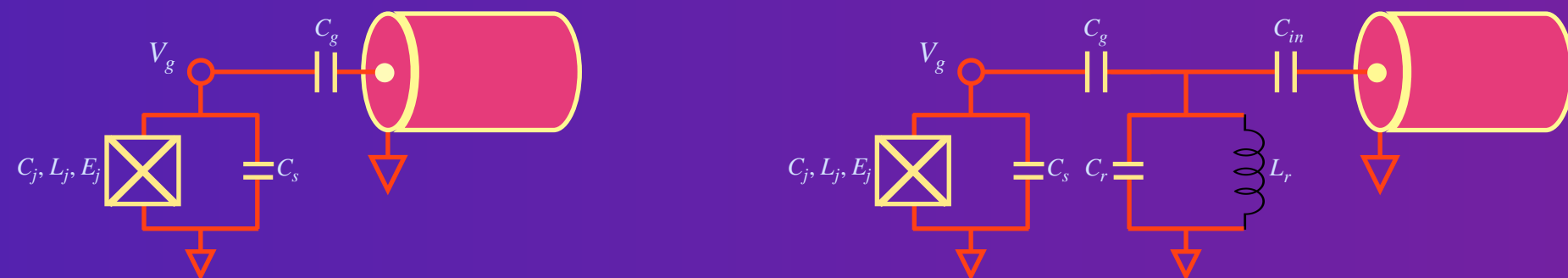
[C Rigetti et al, PRB (2010)]   [JM Chow et al, PRL (2011)]

squared over 2 delta where delta was is the detuning of the difference

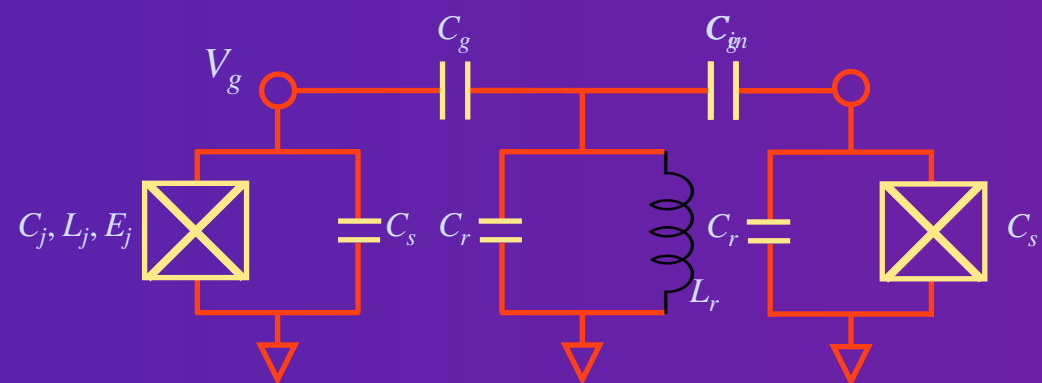
# COUPLING

# KINDS

## QUBIT-CAVITY COUPLING



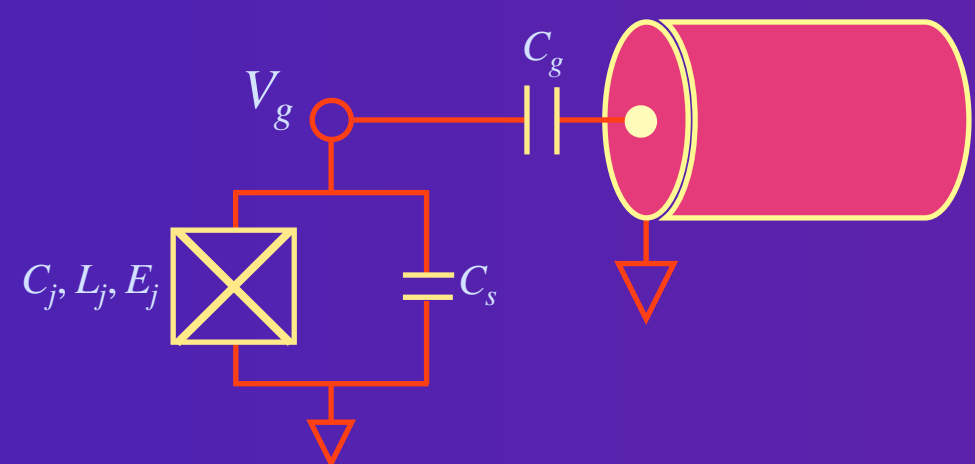
## QUBIT-QUBIT COUPLING



# QUBIT-CAVITY COUPLING

# CIRCUIT SCHEMATIC

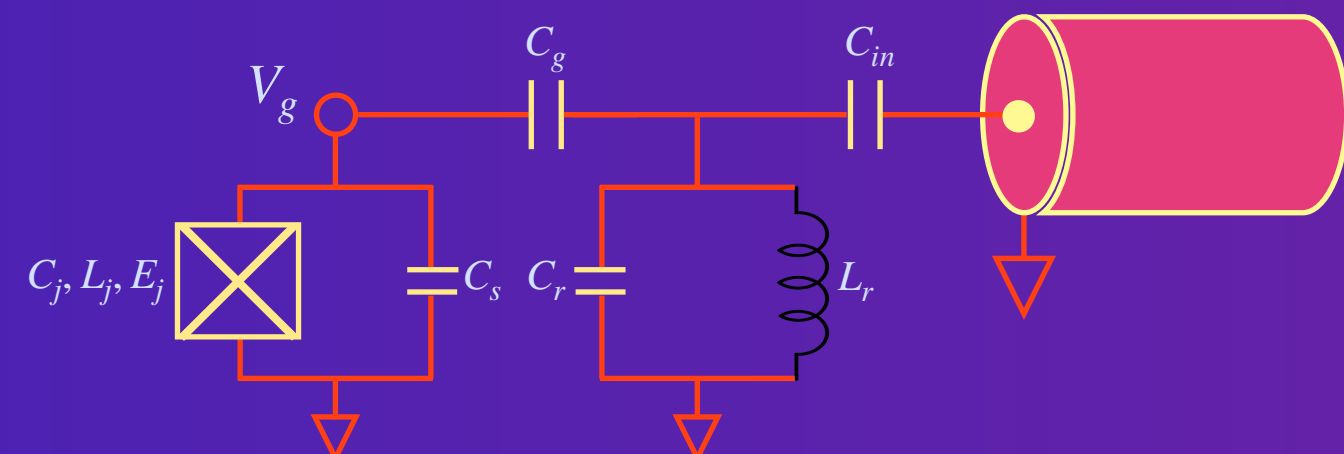
## Direct measurement.



Prone to environmental noise, leading to random bit and phase flip.

Demolition measurements only! Interactions will disturb the state of the system. On resonance regime of cQED.

## Indirect measurement.



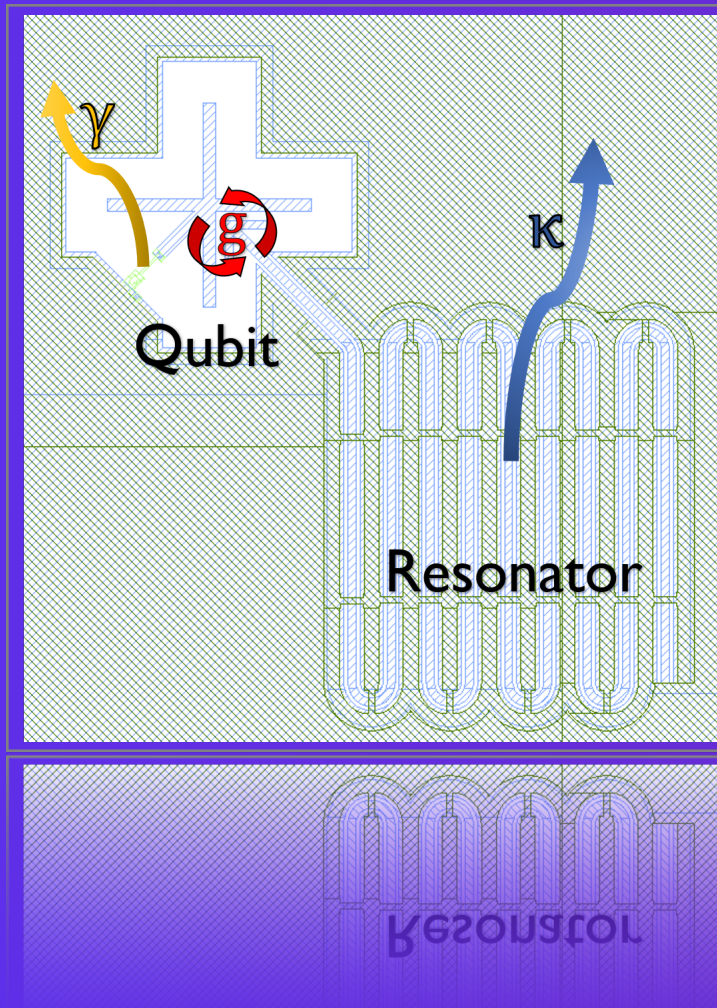
Isolated from noise.

Quantum non-demolition (QND) measurements applied. Enables the dispersive regime of cQED.

# JAYNES-CUMMINGS MODEL

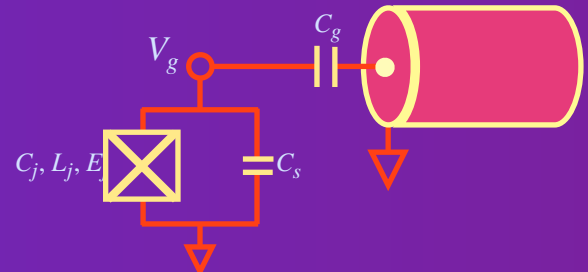
Describes the qubit-cavity interaction between a two-level system (qubit) and a single-mode of an electromagnetic cavity (resonator).

IBM Qiskit.



$$H_{JC}/\hbar = \omega_r(a^\dagger a) + \frac{1}{2}\omega_q\sigma_z + g(a\sigma_+ + a^\dagger\sigma_-)$$

- **Resonator term:** a quantum harmonic oscillator with decay rate  $\kappa$ .
  - **Qubit term:** defines the state of the qubit with spontaneous decay  $\gamma$  due to dissipation.
  - **Interaction term:** describes the electric dipole coupling coupling between the qubit and the cavity with strength  $g$ .
- $\hat{N} = (a^\dagger a)$  is the photon (Fock) number operator operator.
- $\sigma_+ a$  creates a photon in the resonator and lowers the qubit from  $|1\rangle$  to  $|0\rangle$  state, conversely for  $\sigma_- a^\dagger$ .
- $\sigma_\pm$  is the qubit raising/lowering (excitation) operator.
- Strong coupling:**  $g > > \kappa, \gamma$

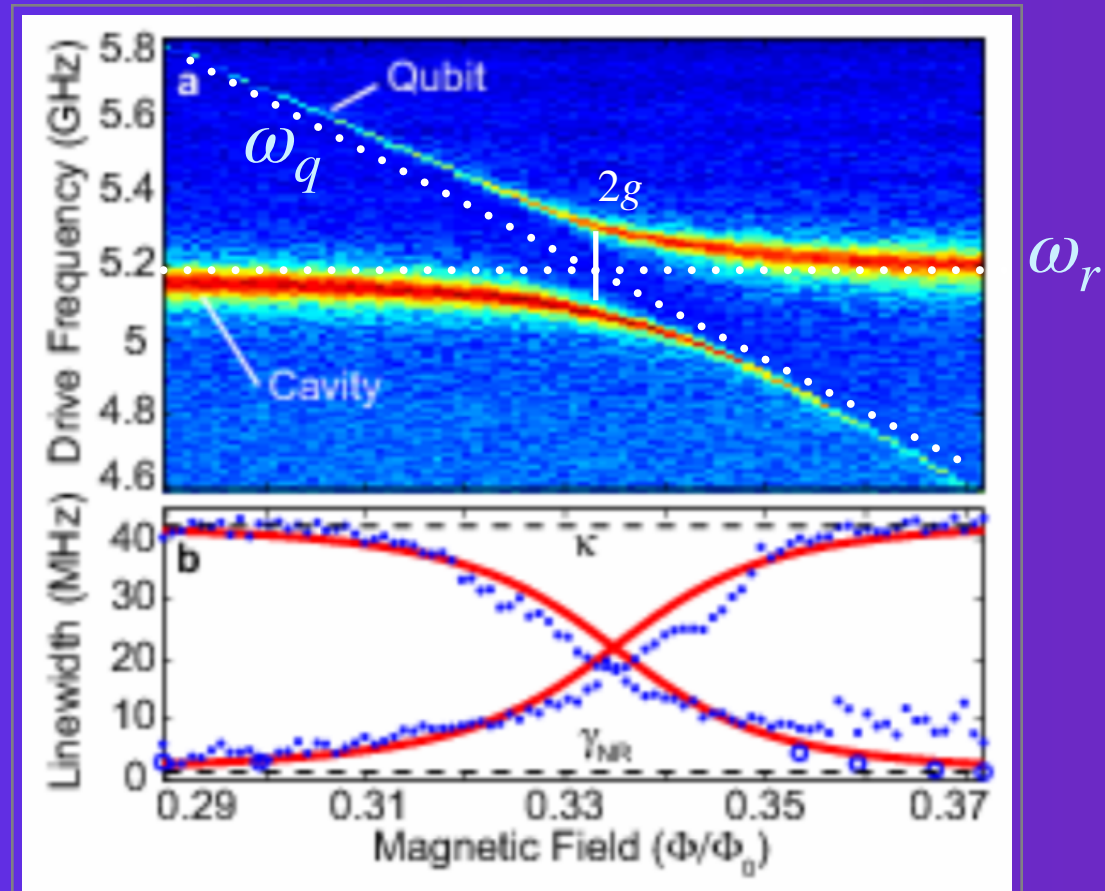


# RABI SPLITTING

On resonance regime

$$\Delta = \omega_q - \omega_r = 0$$

Houck et al., Nature (2007).

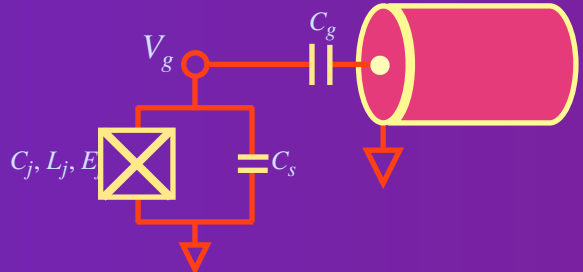


$$H_{int} = \hbar g(a\sigma_+ + a^\dagger\sigma_-)$$

FIG. 2: Enhanced spontaneous emission through the Purcell effect. **a.** Transmission through the cavity-qubit system at different applied fluxes (log scale). Two peaks are evident in transmission due to the vacuum Rabi splitting. Away from the avoided crossing, these peaks correspond to “mostly qubit” and “mostly cavity” states. The bare linewidth of the cavity,  $\kappa/2\pi = 44$  MHz, is much larger than the bare qubit linewidth  $\gamma/2\pi < 2$  MHz. **b.** Extracted linewidths from the data in (a) (closed circles) are compared with theoretical values (red line). As the qubit and cavity peaks approach degeneracy, the qubit peak becomes broader due to spontaneous emission to the cavity mode, while the cavity decay is suppressed. Extra dephasing present only at low frequencies (the right side of the graph) causes a non-Lorentzian line shape and excessive width. Measurements of the relaxation rate in the time domain (open circles) agree with theoretical estimates. Discrepancies arise due to flux instability and variations in non-radiative decay with frequency.

# CALIBRATION

On resonance regime



$|0\rangle$

  $\pi/2$ -pulse

$$|i-\rangle = \frac{|0\rangle - i|1\rangle}{\sqrt{2}}$$

  $\pi/2$ -pulse

Initial state

X90 gate

Superposition

X90 gate

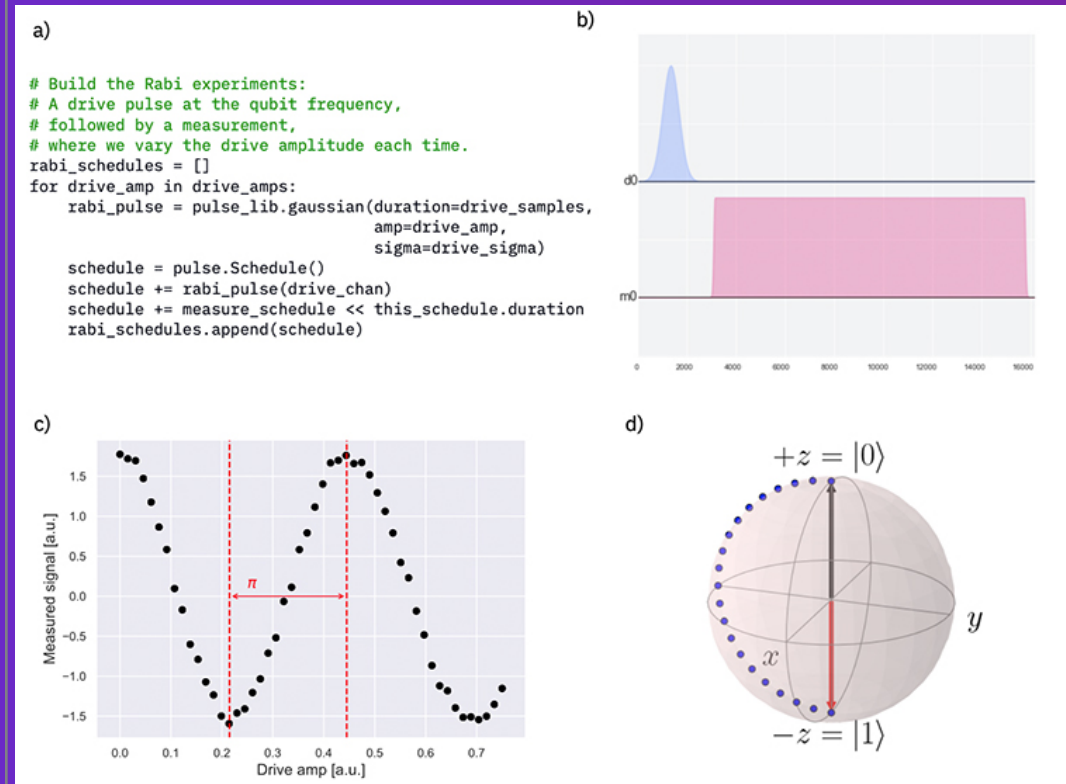
$|0\rangle$

Initial state

  $\pi/2$ -pulse

...

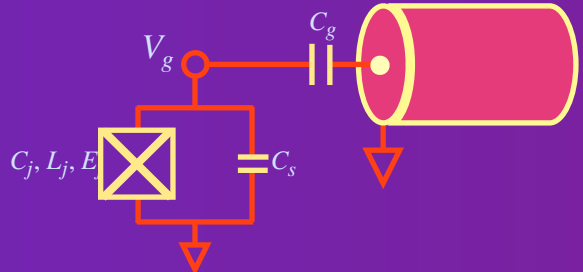
Rabi Experiment [IBM Qiskit].



$$f_{rabi} = \frac{g}{\pi}$$

# RELAXATION TIME ( $T_1$ )

On resonance regime



$|0\rangle$

**Initial state**



$\pi$ -pulse Pauli-X gate

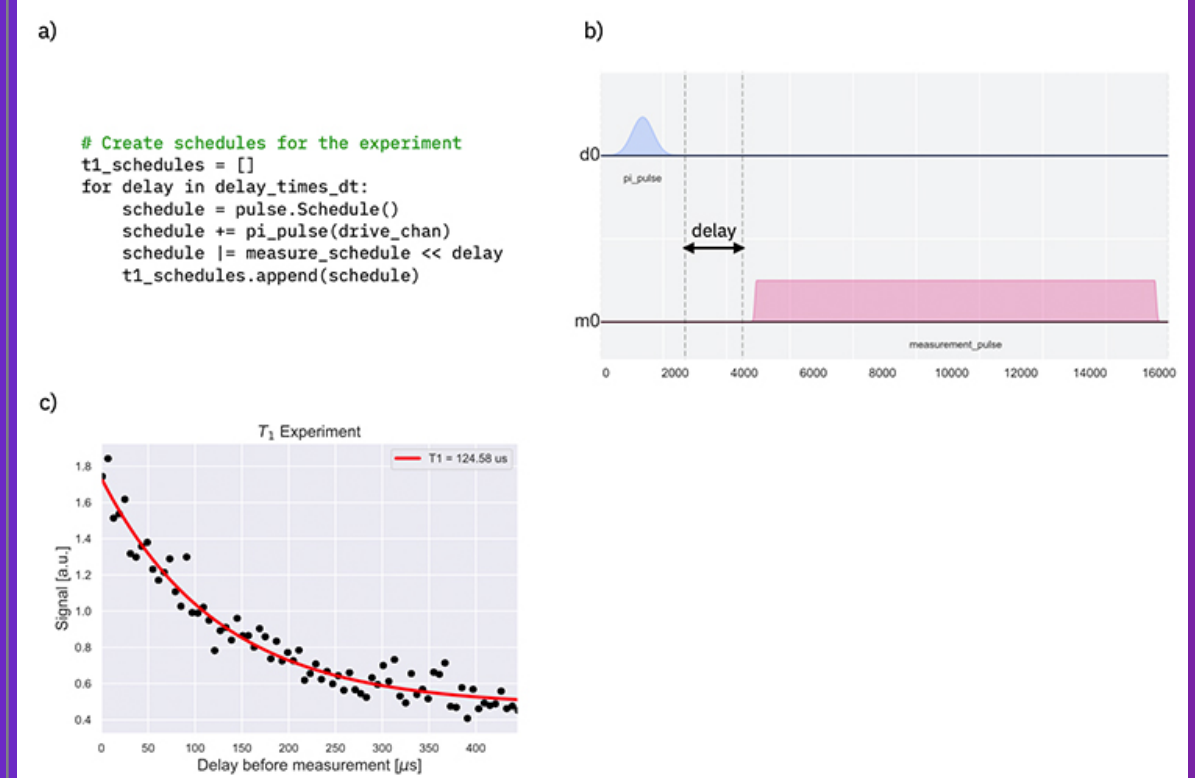
$|1\rangle$

**Excited state**

$|0\rangle$

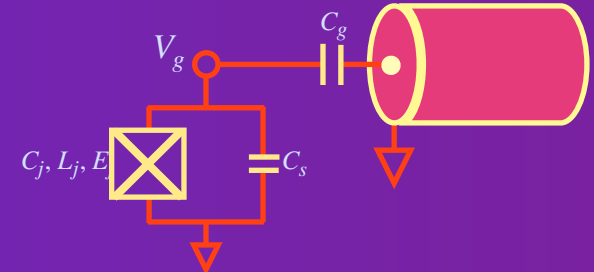
**Exptaneous decay**

PI-pulse Experiment [IBM Qiskit].



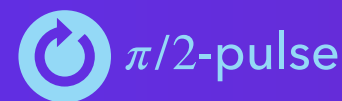
# COHERENCE TIME (T2)

On resonance regime



$|0\rangle$

**Initial state**



$\pi/2$ -pulse

**X90 gate**

$$|i-\rangle = \frac{|0\rangle - i|1\rangle}{\sqrt{2}}$$

**Superposition**



$\pi$ -pulse

**Pauli-X gate**

$$|i+\rangle = \frac{|0\rangle + i|1\rangle}{\sqrt{2}}$$

**Superposition**



$\pi/2$ -pulse

**X90 gate**

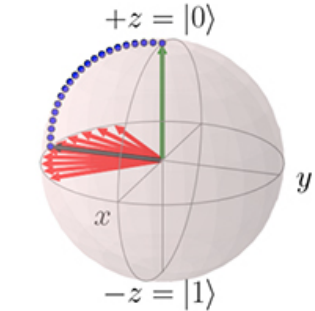
$|0\rangle$

**Final state**

**Hahn echo Experiment [IBM Qiskit].**



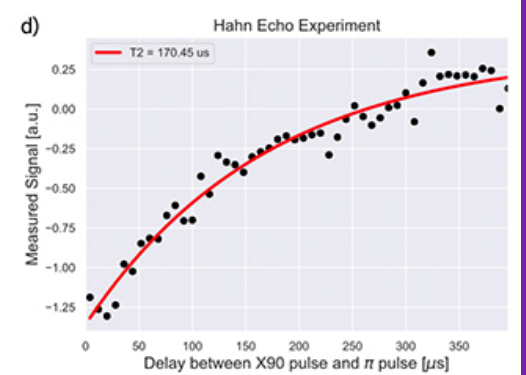
b)



c)

```
t2_schedules = []
for tau in delay_times_dt:
    schedule = pulse.Schedule()
    schedule += x90_pulse(drive_chan)
    schedule += pi_pulse(drive_chan) << tau
    schedule += x90_pulse(drive_chan) << tau
    schedule += measure_schedule << schedule.duration
    t2_schedules.append(schedule)
```

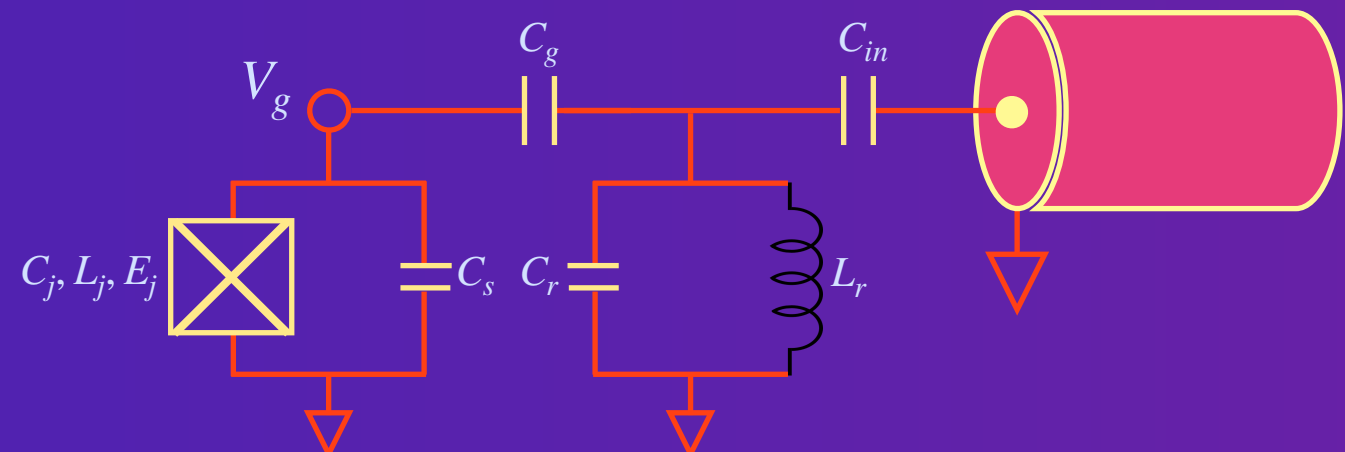
d)



# DISPERSIVE REGIME

$$|\Delta| = |\omega_q - \omega_r| \gg g$$

$$H_{int} = -\hbar\chi\hat{\sigma}_Z a^\dagger a$$



The resonator couples capacitively to a feedline used to determine the scattering properties of the resonator near its fundamental frequency.

# AVOIDED CROSSING

## Dispersive regime

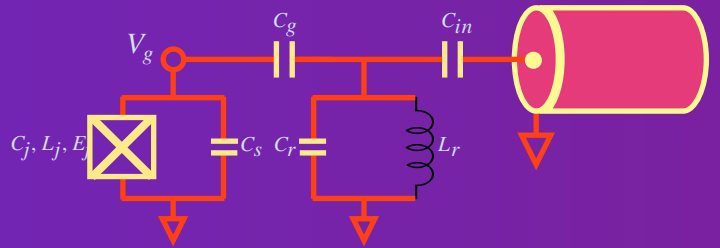
**Driven RWA in the dispersive regime**

$$H_{eff} = \Delta_r a^\dagger a + \sum_j \frac{\Delta_{q,j} + \chi_j}{2} \sigma_j^z + \sum_j \chi_j a^\dagger a \sigma_j^z + (a \xi^* + a^\dagger \xi)$$



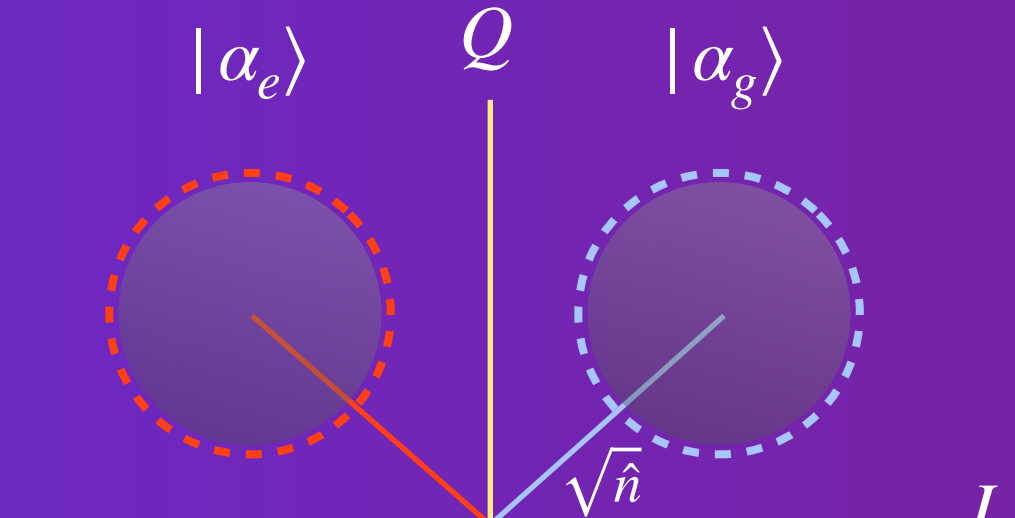
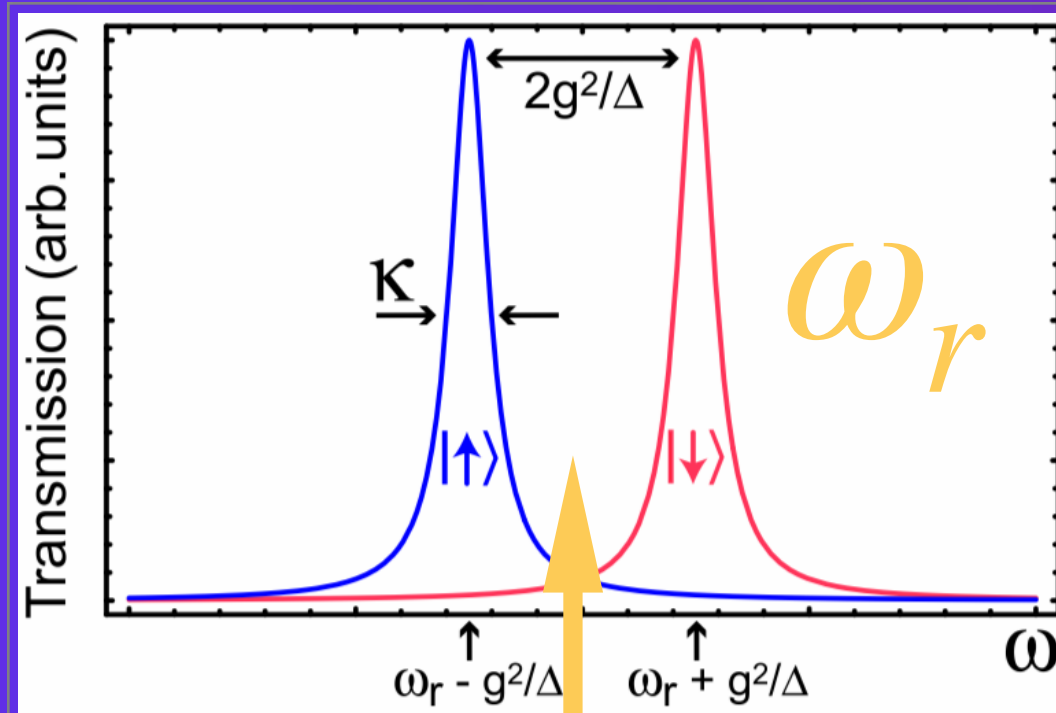
# JAYNES-CUMMINGS

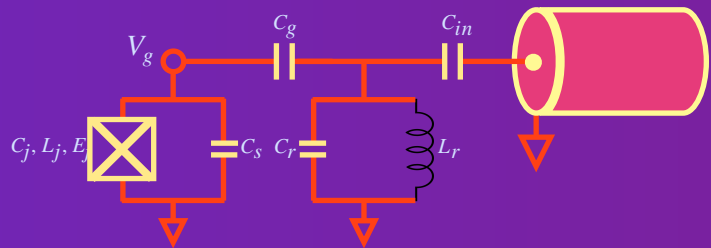
## Dispersive regime



$$2\chi = 2g^2/\Delta$$

Blais et al. [2004].





# DICKE MODEL

## N-qubit-cavity coupling

The Dicke model describes the coupling between a single-mode cavity and N spin- $\frac{1}{2}$  degrees of freedom (two-level systems a.k.a qubits).

### Tavis-Cummings Hamiltonian

$$H = \omega_r a^\dagger a + \sum_j \frac{\omega_{q,j}}{2} \sigma_j^z + \sum_j g_j (a \sigma_j^+ + a^\dagger \sigma_j^-) + (a \xi^* e^{i\omega_d t} + a^\dagger \xi e^{-i\omega_d t})$$

### Dispersive Regime in the RWA

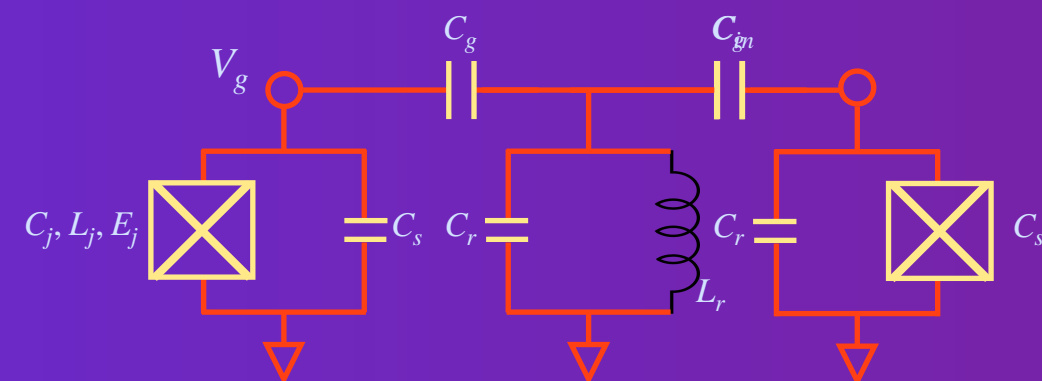
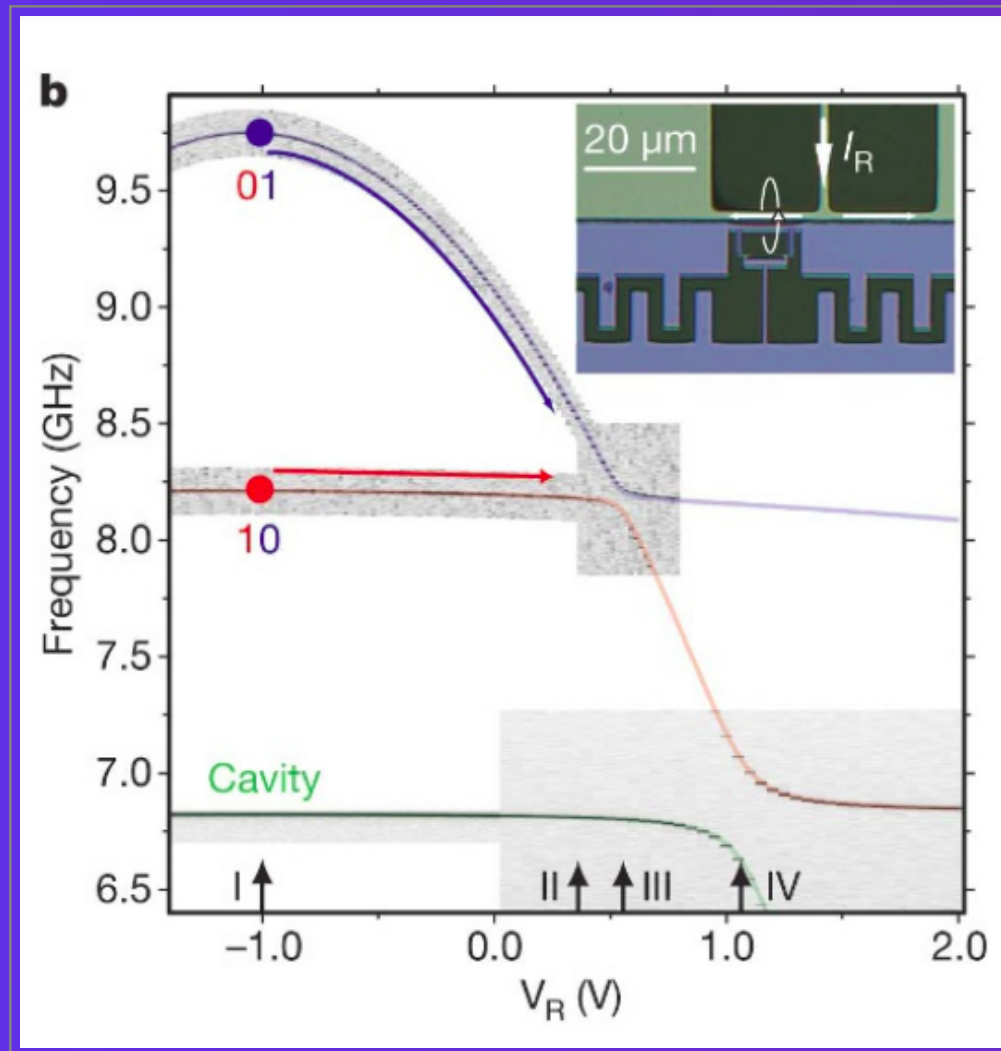
$$H_{eff} = \Delta_r a^\dagger a + \sum_j \frac{\Delta_{q,j} + \chi_j}{2} \sigma_j^z + \sum_j \chi_j a^\dagger a \sigma_j^z + (a \xi^* + a^\dagger \xi)$$

# QUBIT-QUBIT COUPLING

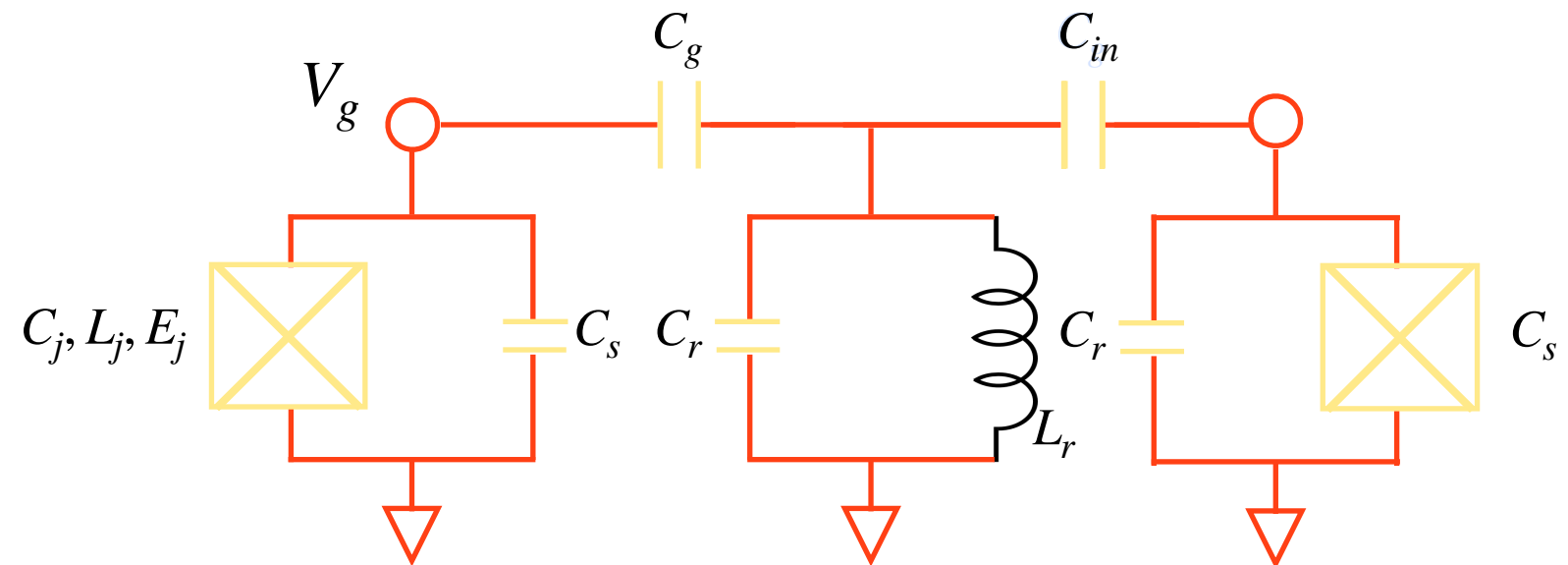
# QUBIT-QUBIT COUPLING

2-qubit gates (e.g, CNOT for Entanglement)

DiCarlo et al., Nature 2009.



When the interaction between two qubits is mediated by a dispersively coupled common bus resonator there is still an avoided crossing when one qubit is tune through resonance with the other qubit.

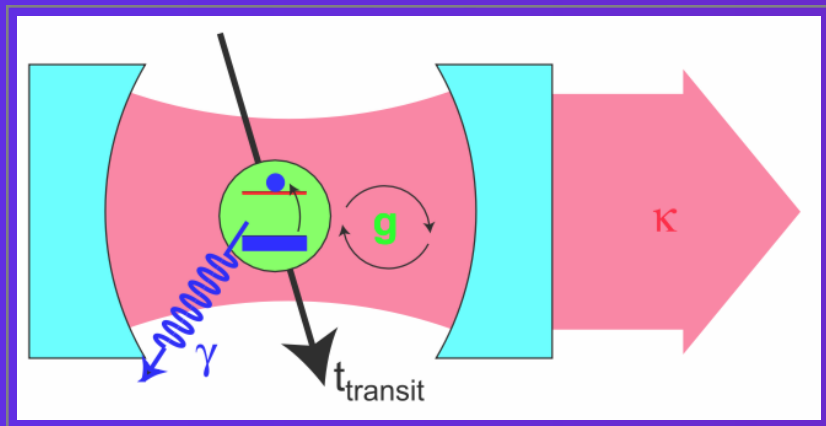


# PROCESSOR DESIGN

# SINGLE READOUT

Full wave CPW  $\lambda = 1$ .

Blais et al., 2004.



$$\omega_r/2\pi = 10\text{GHz} \quad (h\nu/k_B \sim 0.5\text{K})$$

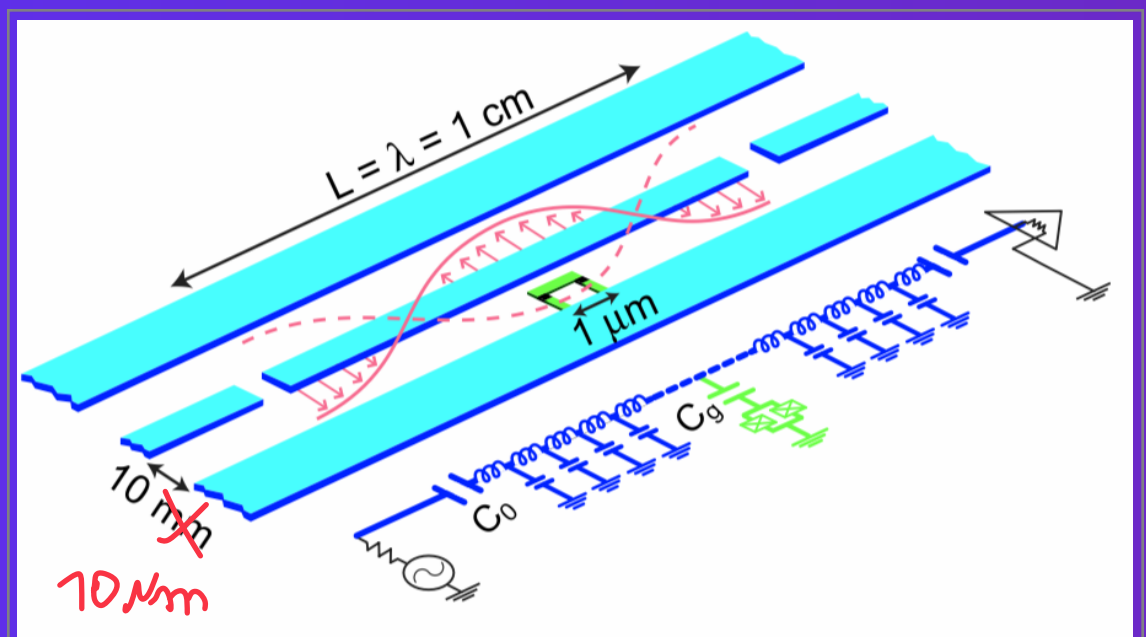
$$\beta = C_g/C_\Sigma = 0.1$$

$$V_{rms}(t) = \sqrt{\hbar\omega_r/C_l L} \approx 2\mu\text{V}$$

$$g/\pi = \frac{1}{\pi} \frac{\beta e}{\hbar} \sqrt{\frac{\hbar\omega_r}{C_l L}} = 100\text{MHz}$$

$$d = 2 \times 10^4 \text{au}$$

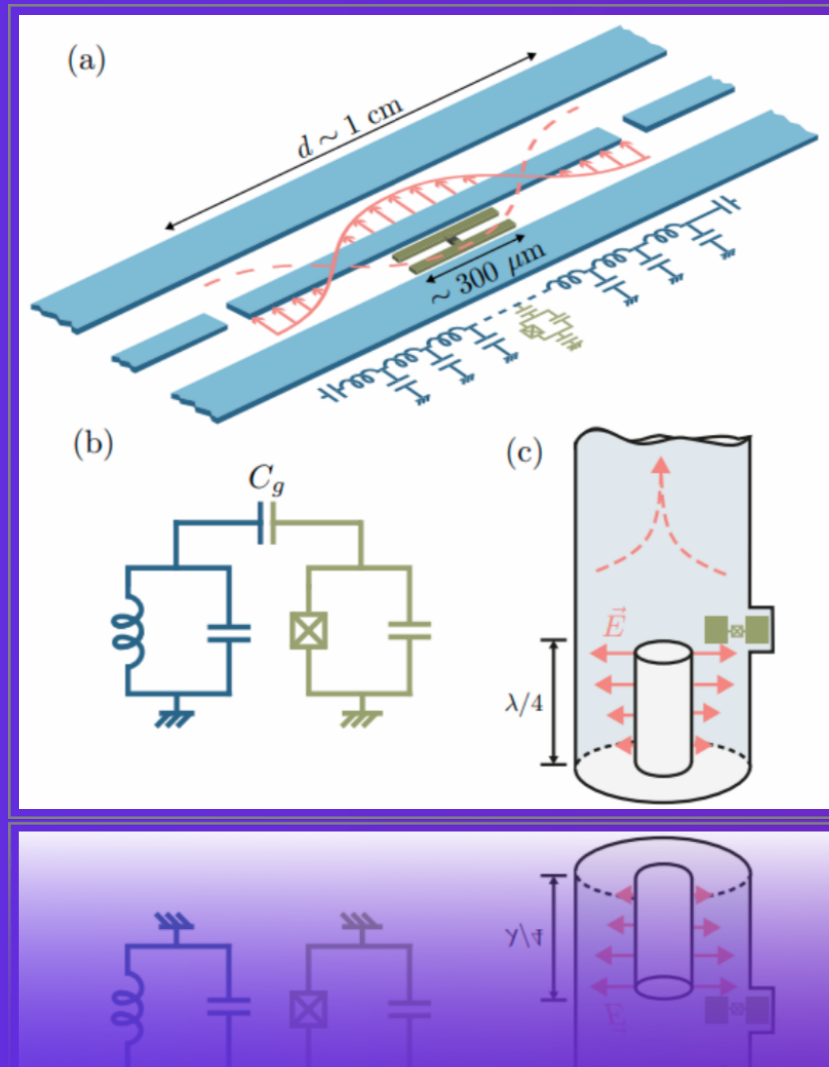
$$\epsilon_{rms} = \hbar g/d = 0.2\text{V/m}$$



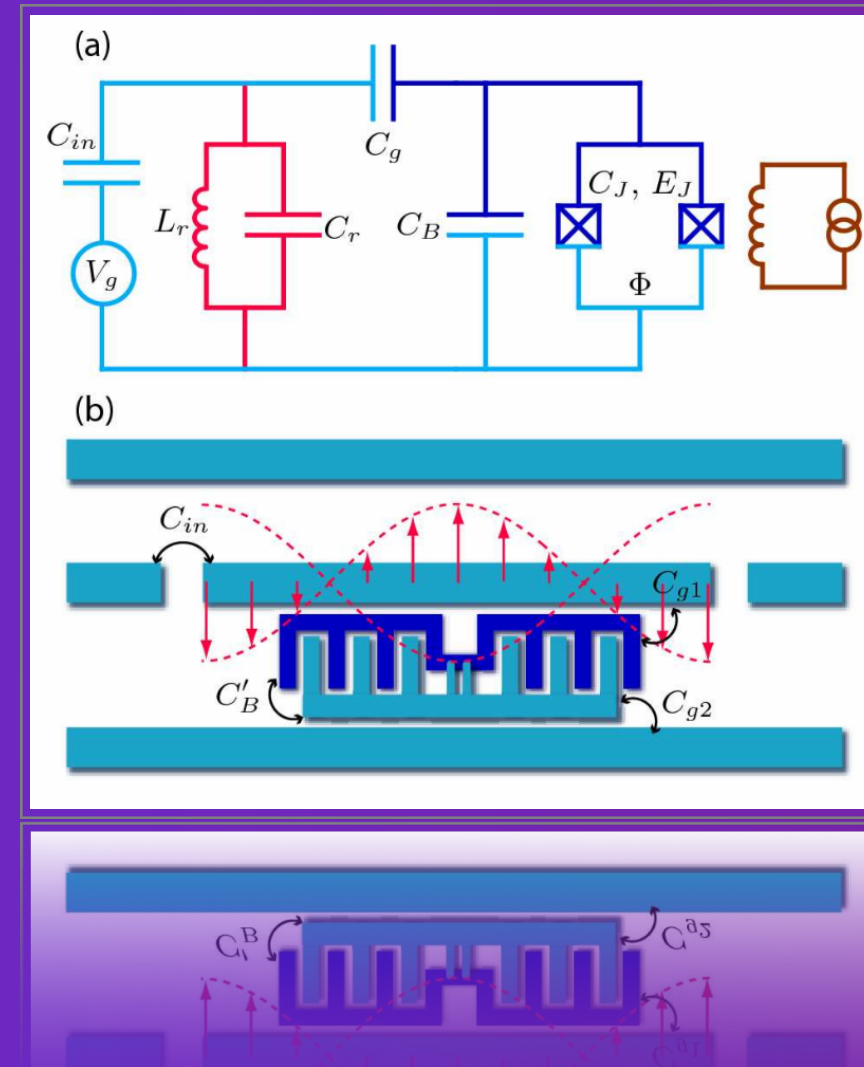
# SINGLE READOUT

Full wave CPW  $\lambda = 1$ .

A. Blais et al., 2020.



A. Blais et al., 2020.



# FOUR-PORT TWO-QUBIT PROCESSOR

Houck et al., Nature 2007.

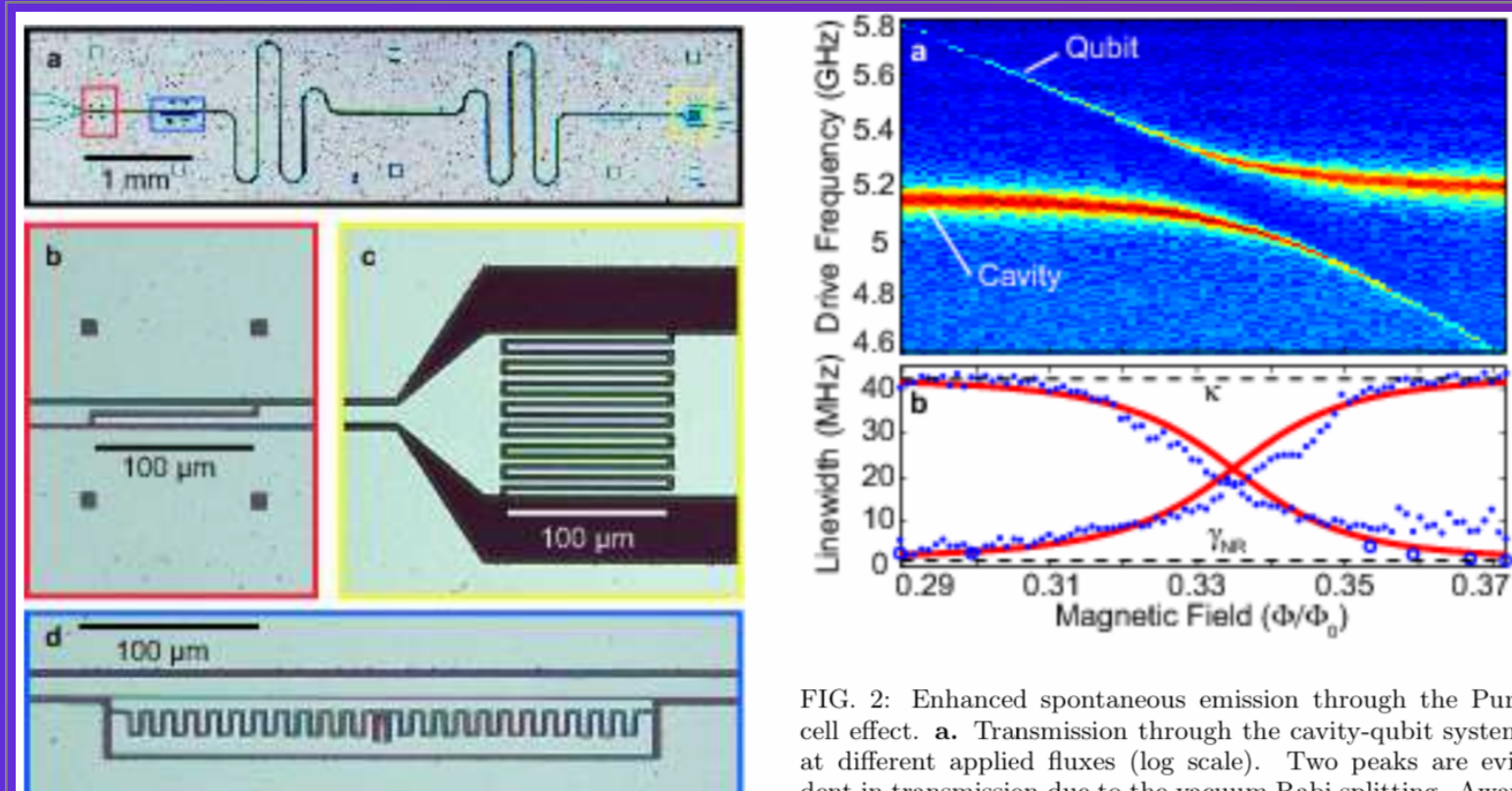


FIG. 1: The circuit QED device for generating single photons. **a.** A transmission line cavity is formed between two capacitors, with the input capacitor shown in **b** and the output in **c**. Because the output is much larger, most radiation leaving the cavity leaves from this port, allowing efficient collection of light emitted from the cavity. **d.** Transmon qubit, an optimized Cooper Pair Box, at a voltage anti-node of the cavity. The qubit is characterized by a Josephson energy, tuned by an applied magnetic field with a maximum of  $E_J^{\max} = 20.2$  GHz and a charging energy  $E_c = 0.37$  GHz. The coupling to the cavity is  $g = 107$  MHz at the qubit frequency primarily used in this paper,  $\omega_a = 4.68$  GHz, and has a slight dependence on the qubit frequency.

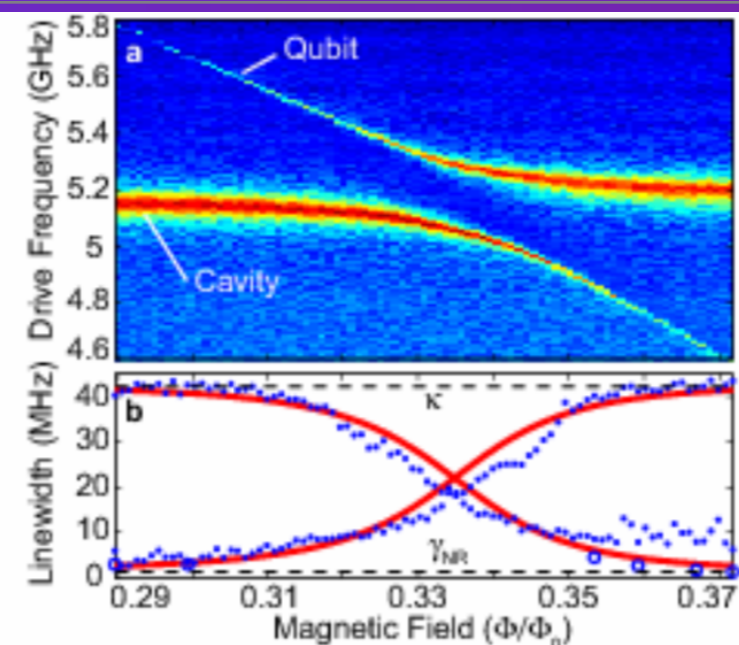
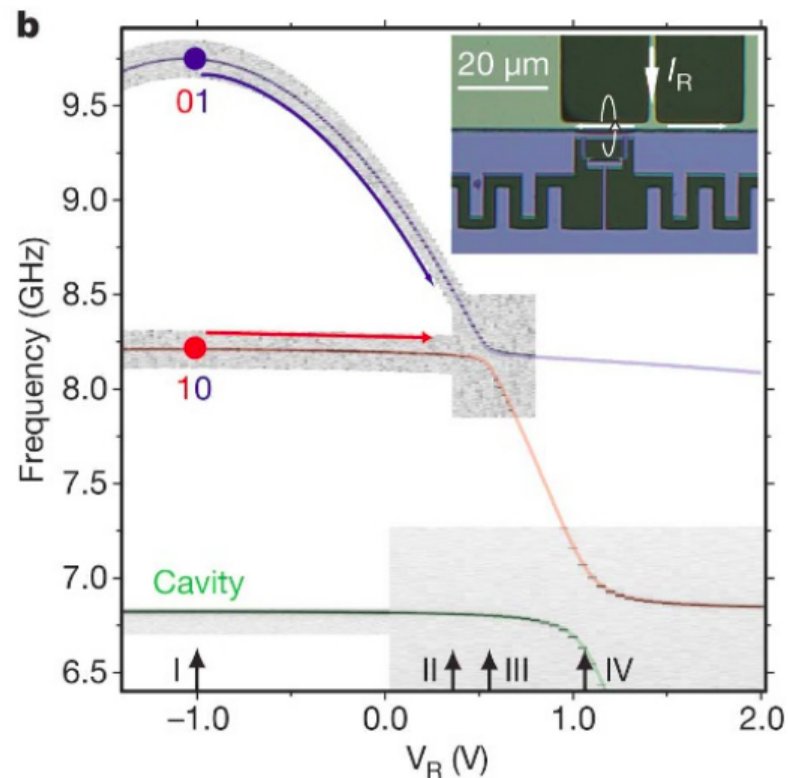
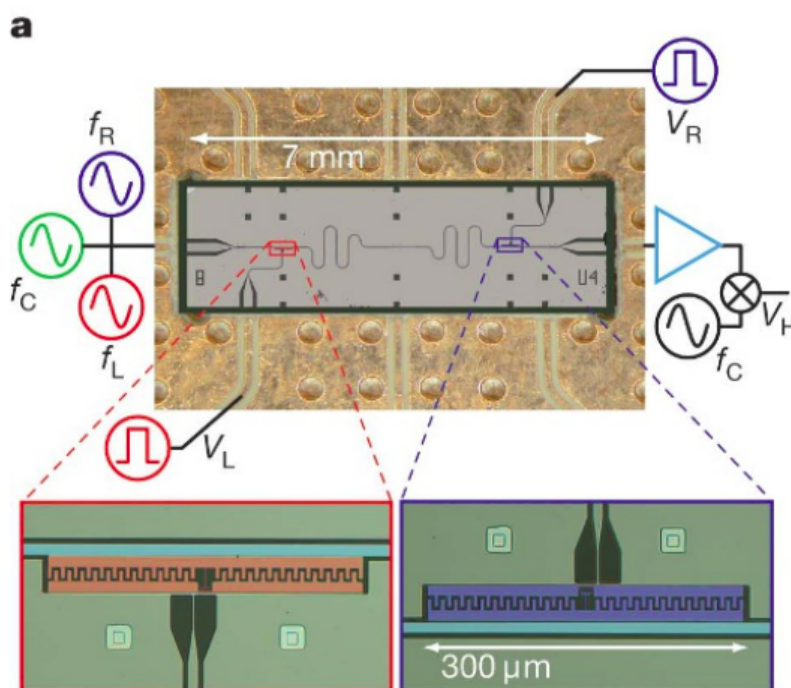


FIG. 2: Enhanced spontaneous emission through the Purcell effect. **a.** Transmission through the cavity-qubit system at different applied fluxes (log scale). Two peaks are evident in transmission due to the vacuum Rabi splitting. Away from the avoided crossing, these peaks correspond to “mostly qubit” and “mostly cavity” states. The bare linewidth of the cavity,  $\kappa/2\pi = 44$  MHz, is much larger than the bare qubit linewidth  $\gamma/2\pi < 2$  MHz. **b.** Extracted linewidths from the data in (a) (closed circles) are compared with theoretical values (red line). As the qubit and cavity peaks approach degeneracy, the qubit peak becomes broader due to spontaneous emission to the cavity mode, while the cavity decay is suppressed. Extra dephasing present only at low frequencies (the right side of the graph) causes a non-Lorentzian line shape and excessive width. Measurements of the relaxation rate in the time domain (open circles) agree with theoretical estimates. Discrepancies arise due to flux instability and variations in non-radiative decay with frequency.

# FOUR-PORT TWO-QUBIT PROCESSOR

DiCarlo et al., Nature 2009.

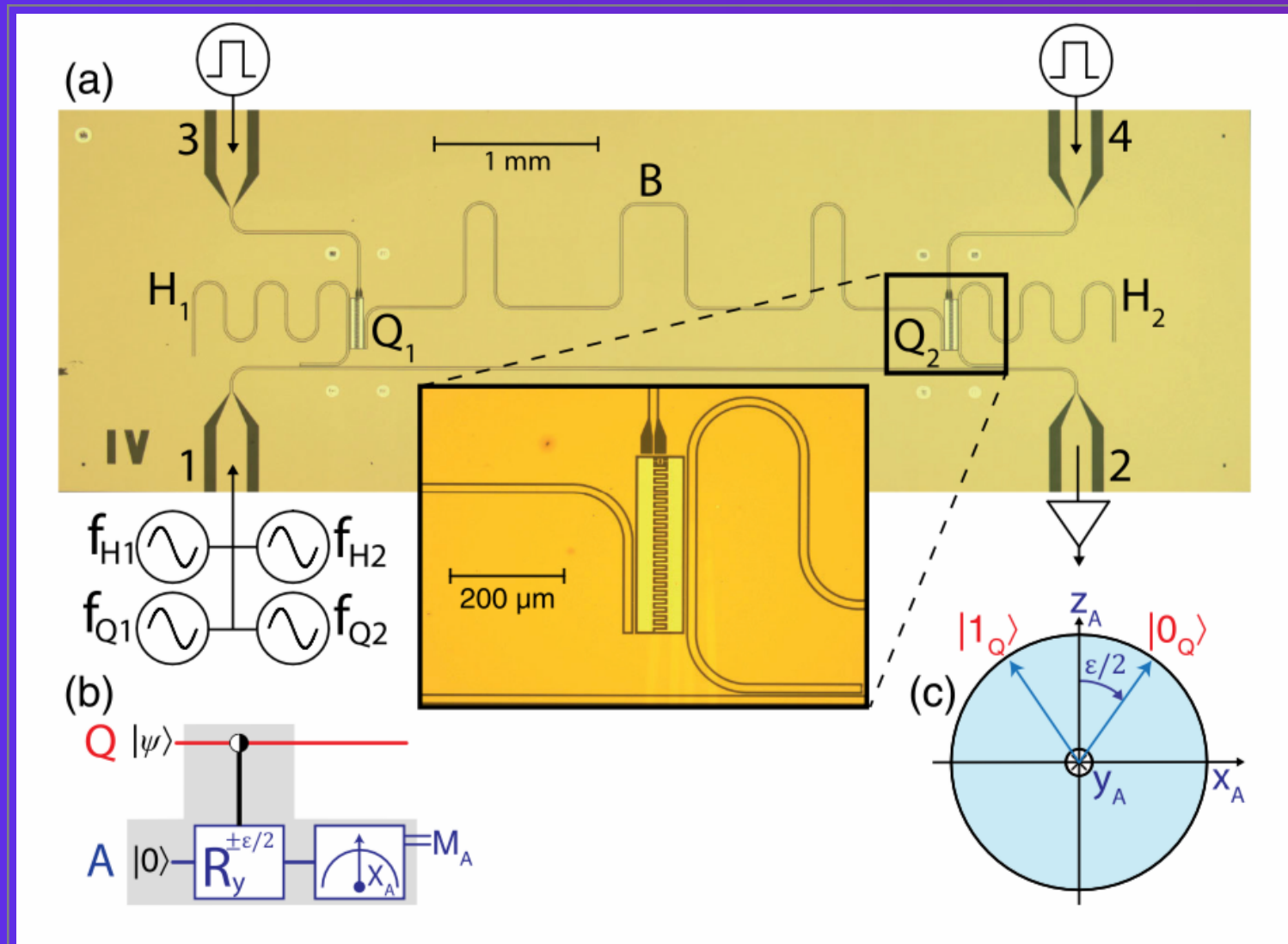


- ▶ Two transmon qubits;
- ▶ One resonator:  
with capacitive termination at  
both ends, i.e, half-  
wave ( $\lambda/2$ ) resonator;
- ▶ Two flux lines, one per qubit.



# FOUR-PORT TWO-QUBIT PROCESSOR

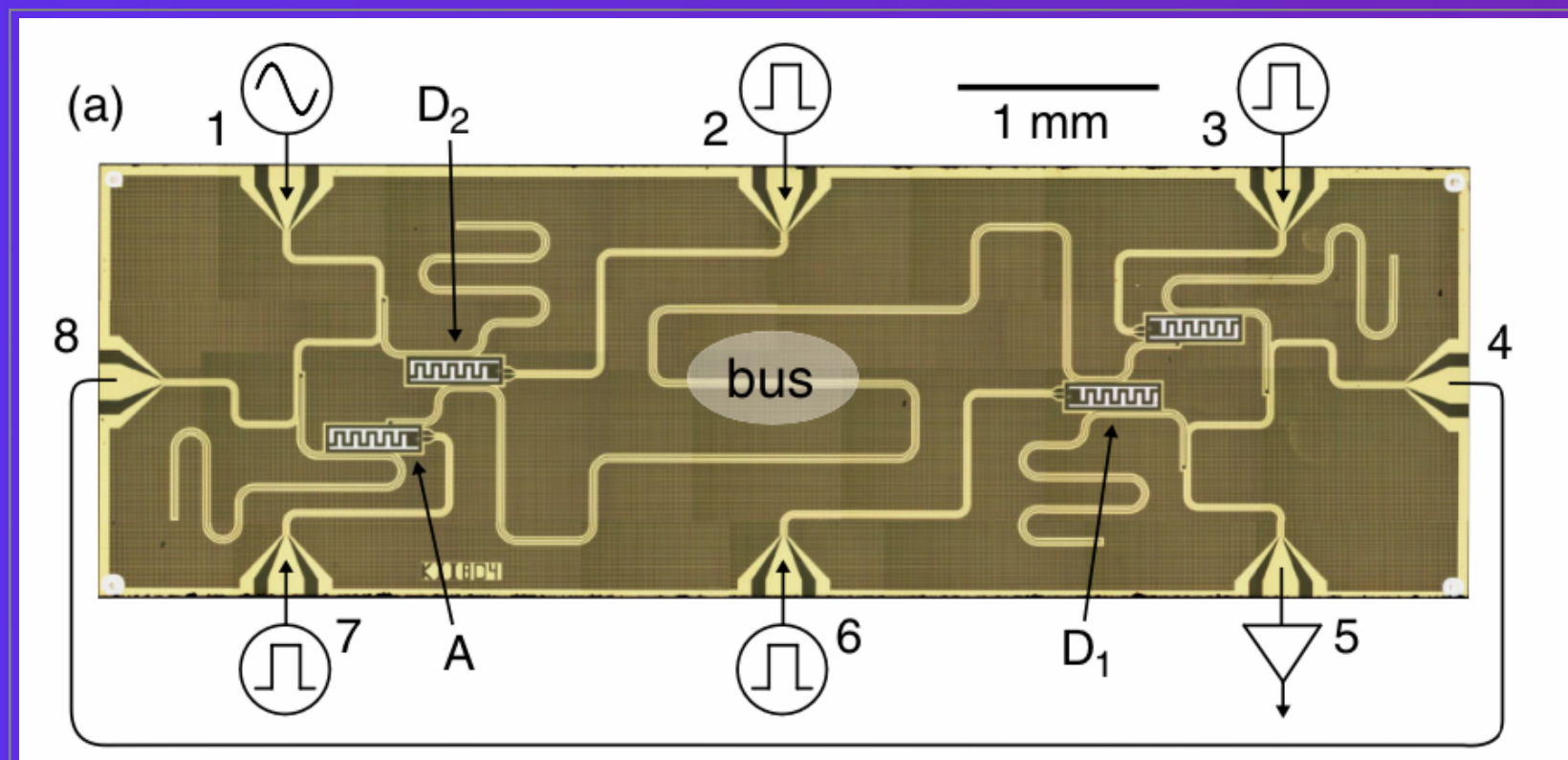
Groen et al., Phys. Rev. Lett., 2013.



- ▶ Two transmon qubits;
- ▶ One half-wave ( $\lambda/2$ ) bus resonator in the middle;
- ▶ Two  $\lambda/4$  readout resonators (one per qubit) coupled to a common feedline.
- ▶ Two flux lines, one per qubit.

# EIGHT-PORT FOUR-QUBIT PROCESSOR

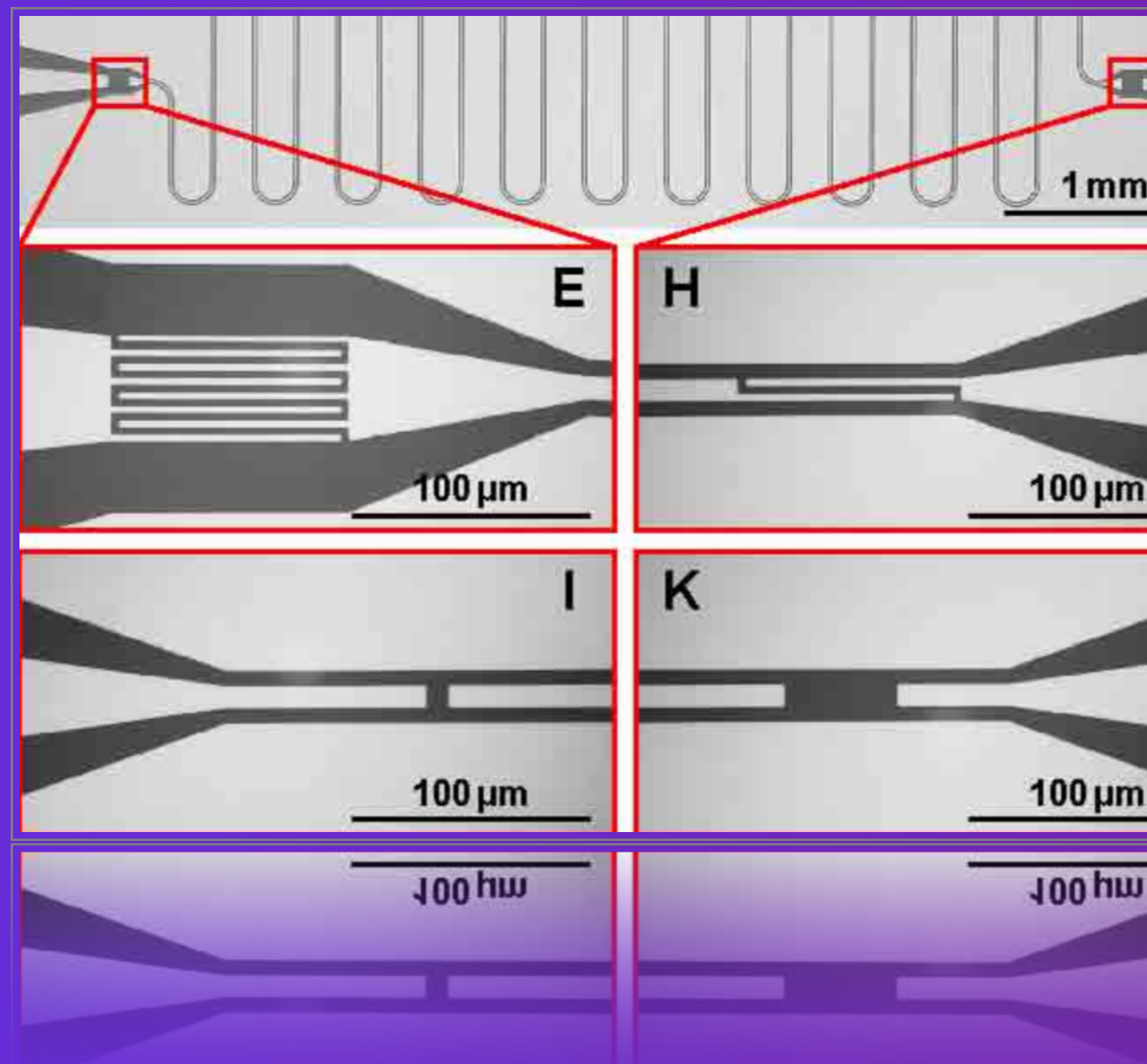
Saira et al., Phys Rev. Lett., 2014.



- Four transmon qubits;



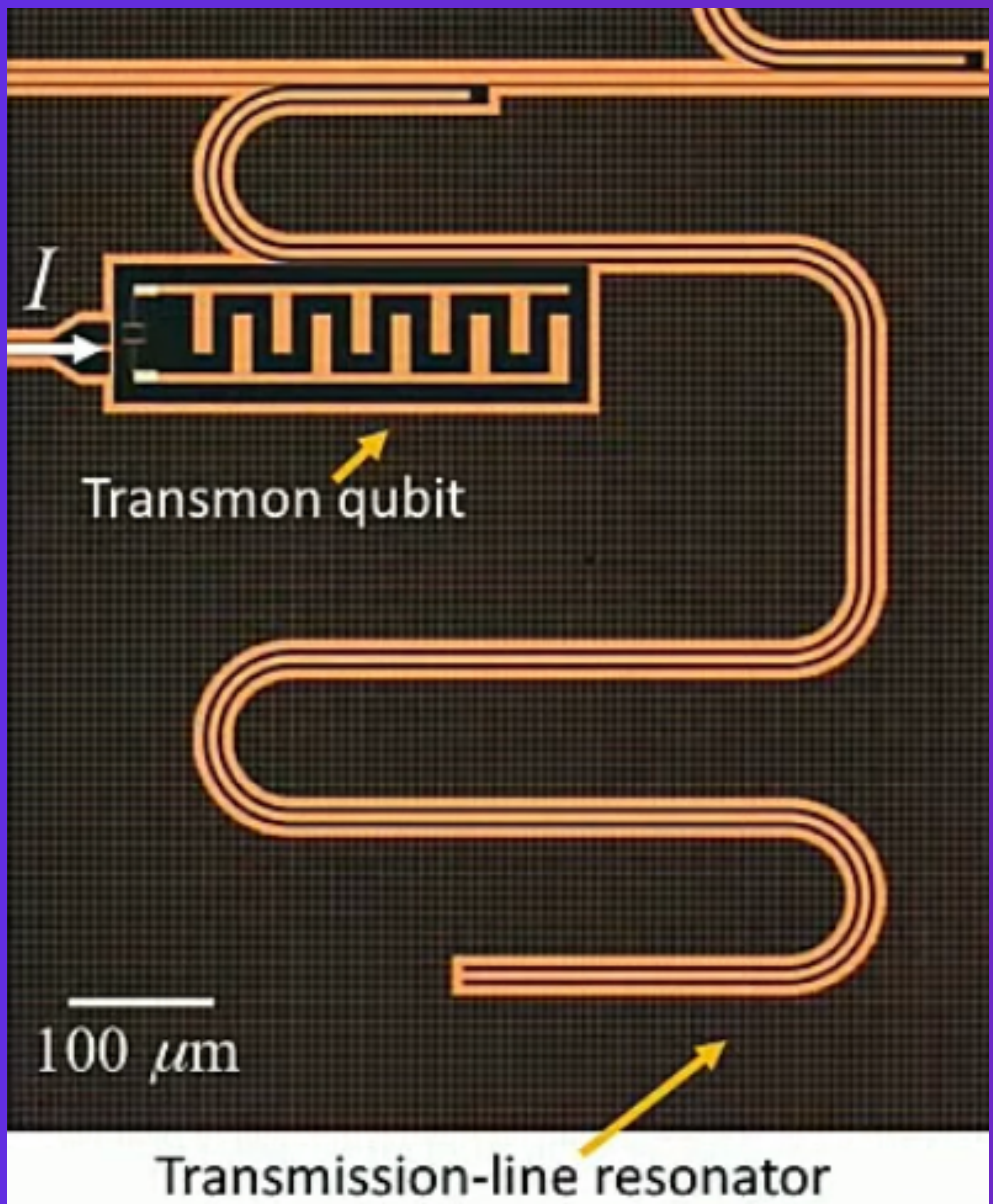
# INTERCONNECTS



M. Goppl et al., 2008.

# INTERCONNECTS

QuTech [2018].



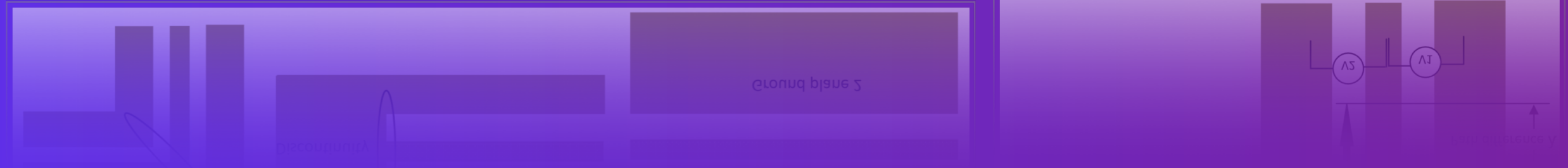
The resonator has:

- ▶ i) a short circuit termination at the far end;
- ▶ ii) an open circuit termination at the close end that couples capacitively to a feedline used to determine the scattering properties of the resonator near its fundamental frequency.

# INTERCONNECTS

## Bending, discontinuity, and asymmetry

M. Abuwasib [Thesis].

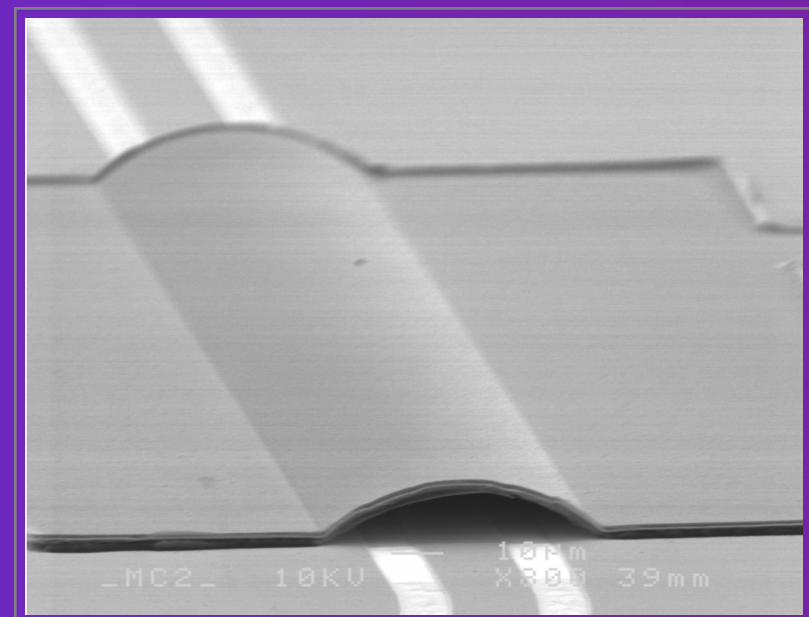
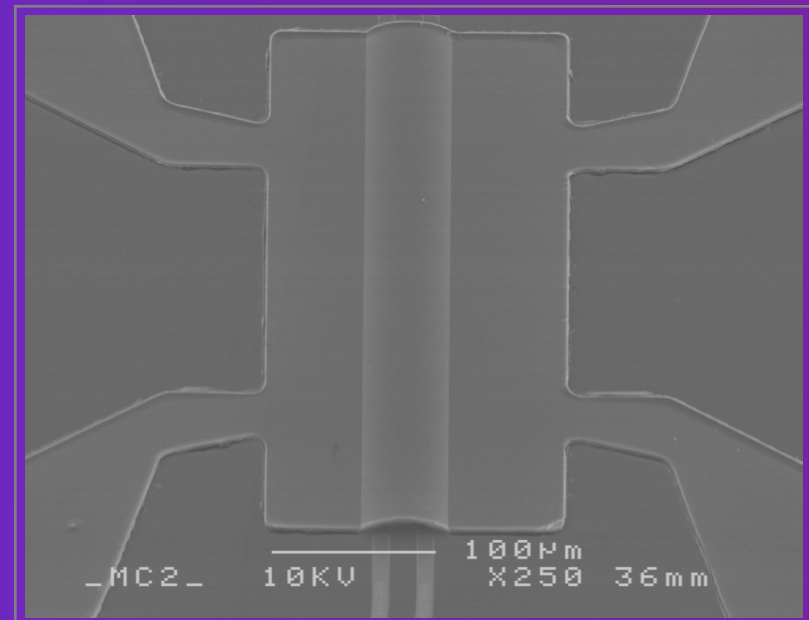
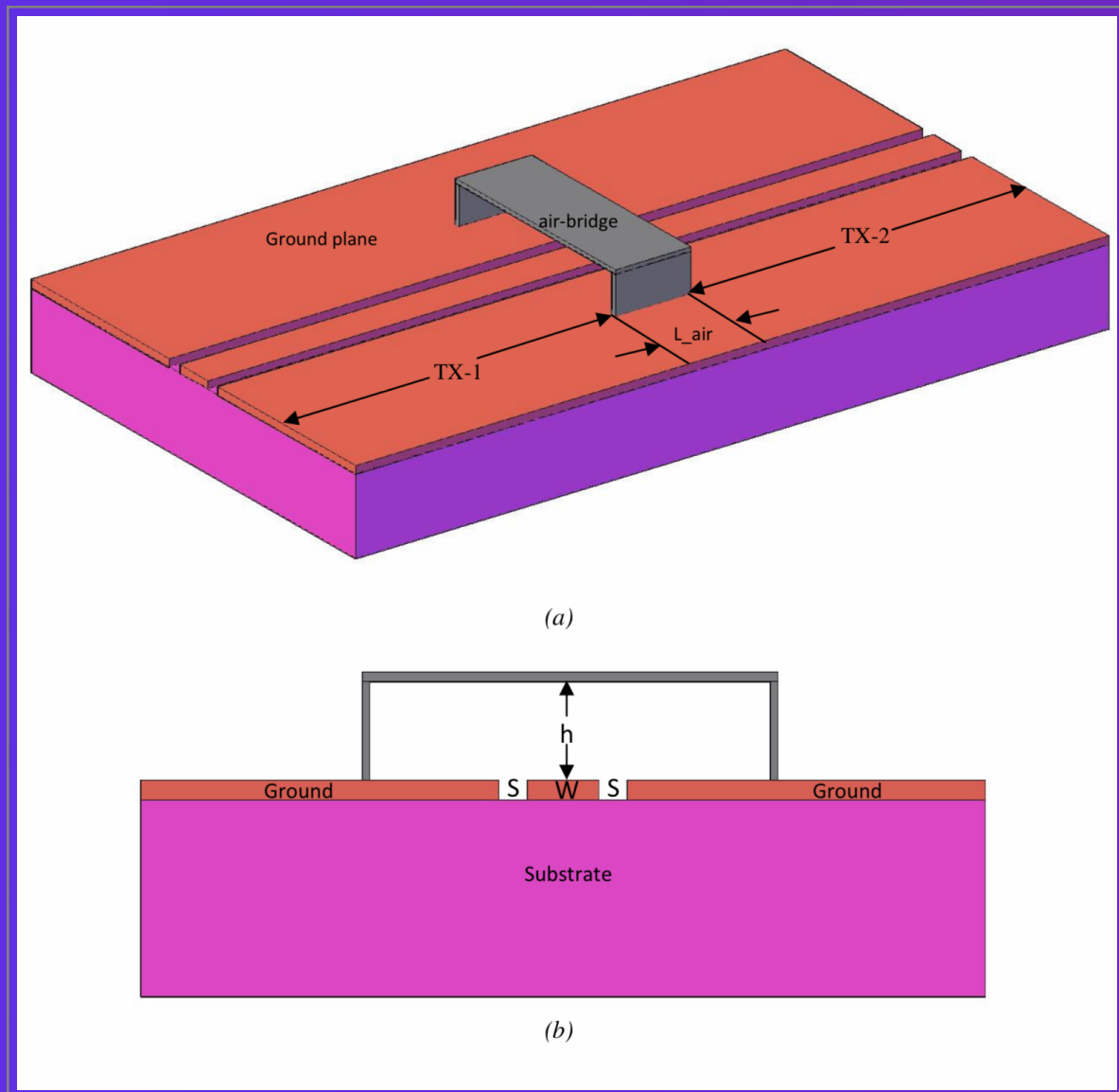


# INTERCONNECTS

## Air-bridge crossover

M. Abuwasib [2013].

M. Abuwasib [Thesis].



THANK YOU

多謝~~

# REFERENCES

M. Tinkham, "Introduction to Superconductivity", McGraw-Hill.

"Microwave Engineering," by David Pozar, 4th ed. (2012).

M. Goppl et al., "Coplanar Waveguide Resonators for Circuit Quantum Electrodynamics," 2008.

M. H. Devoret, A. Wallraff, and J. M. Martinis, "Superconducting Qubits: a short review," 2004.

J. Koch et al., "Charge-insensitive qubit design derived from the Cooper pair box," Phys. Rev. A 76.4, p. 042319 (2007).

Blais et al., "circuit Quantum Electrodynamics," 2020.

Houck et al., "Generating Single Microwave Photons in a Circuit," 2007.

Blais et al., "Cavity quantum electrodynamics for superconducting electrical circuits: An architecture for quantum computation," 2004.

M. Abuwasib et al., "Fabrication of large dimension aluminum air-bridges for superconducting quantum circuits," 2013.

# REFERENCES

Jongjoo Lee, Heeseok Lee, Woopoung Kim, Jaehoon Lee, Joungho Kim, "Suppression of coupled-slotline mode on CPW using air-bridges measured by picoseconds photoconductive sampling", IEEE microwave and guided wave letters, Vol. 9, No. 7, July 1999.